# Radiation Stability of Cations in Ionic Liquids. 2. Improved Radiation Resistance Through Charge Delocalization in 1-Benzylpyridinium.

**ARTICLE** *in* THE JOURNAL OF PHYSICAL CHEMISTRY B · OCTOBER 2013

Impact Factor: 3.3 · DOI: 10.1021/jp408242b · Source: PubMed



**6 AUTHORS**, INCLUDING:

Ilya Shkrob
Argonne National Laboratory
**143** PUBLICATIONS **2,164** CITATIONS
SEE PROFILE

Timothy W Marin
Benedictine University
**54** PUBLICATIONS **810** CITATIONS
SEE PROFILE

James Wishart
Brookhaven National Laboratory
**115** PUBLICATIONS **3,642** CITATIONS
SEE PROFILE

THE JOURNAL OF PHYSICAL CHEMISTRY B

Article

pubs.acs.org/JPCB

# Radiation Stability of Cations in Ionic Liquids. 2. Improved Radiation Resistance through Charge Delocalization in 1-Benzylpyridinium

Ilya A. Shkrob,*[,†] Timothy W. Marin,[†,‡] Jasmine L. Hatcher,[§,⊥] Andrew R. Cook,[§] Tomasz Szreder,[§,∥,#] and James F. Wishart[§]

[†]Chemical Sciences and Engineering Division, Argonne National Laboratory, 9700 South Cass Avenue, Argonne, Illinois 60439, United States

[‡]Chemistry Department, Benedictine University, 5700 College Road, Lisle, Illinois 60532, United States

[§]Chemistry Department, Brookhaven National Laboratory, Upton, New York 11973-5000, United States

[∥]Department of Radiation Chemistry and Technology, Institute of Nuclear Chemistry and Technology, Dorodna 16, 03-195 Warsaw, Poland

Supporting Information

**ABSTRACT:** Hydrophobic room-temperature ionic liquids (ILs) hold promise as replacements for molecular diluents for processing of used nuclear fuel as well as for the development of alternative separations processes, provided that the solvent can be made resistant to ionizing radiation. We demonstrate that 1-benzylpyridinium cations are uniquely suited as radiation resistant cations due to the occurrence of charge delocalization in both their reduced and oxidized forms in the ILs. It is suggested that the excess electron and hole in the latter ILs are stabilized through the formation of $\pi$-electron sandwich dimers that are analogous to the well-known dimer radical cations of aromatic molecules. This charge delocalization dramatically reduces the yield of fragmentation by deprotonation and the loss of benzyl arms, thereby providing a synthetic path to radiation resistant ILs that are suitable for nuclear fuel processing.

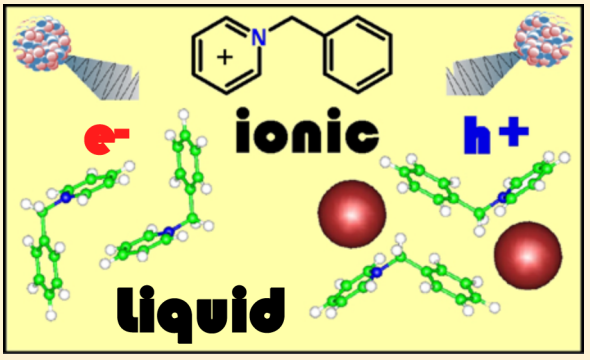


## 1. INTRODUCTION

The motivation to improve the radiation stability of constituent cations in hydrophobic ionic liquid (IL) diluents to be used in nuclear separations and the related radiation chemistry issues have been discussed in part 1.[1] Examination of this chemistry suggested that suppressing the elimination of aliphatic side arms from radiolytically generated, electronically excited cations might be difficult to achieve, as this reaction is inherently irreversible. It was suggested that using cations ($BR^+$) with arms (R) that can yield stable carbocations,[2] such as benzyl (Bz), might be preferable, as the dissociation can become reversible.

$$\{BR^+\}^{**} \rightarrow B + R^+ \quad (1a)$$

$$B + R^+ \rightarrow BR^+ \quad (1b)$$

in contrast to the elimination of the aliphatic arm

$$\{BR^+\}^{**} \rightarrow BH^+ + R(-H) \quad (2)$$

to produce the corresponding 1-olefin. It was shown in part 1[1] that this strategy largely fails for 5-atom heterocycle bases such as imidazolium and 1,2,4-triazolium, as the electron attachment becomes dissociative, resulting in the elimination of stable benzyl radicals ($R^\bullet$)

$$BR^+ + e^{-\bullet} \rightarrow BR^\bullet \quad (3a)$$

$$BR^\bullet \rightarrow B + R^\bullet \quad (3b)$$

Reactions analogous to reaction 3b are also known to occur for $R_3NBz^+$ cations reduced by hydrated electron in water.[3,4] The only exception we found was 1-benzyl-5-methylthiazolium cations, but their electronically excited states proved to be unstable, making them unsuitable for applications where radiation stability is important.

In this study, we demonstrate that 1-benzylpyridinium ($BzPy^+$) cations in ILs undergo reaction 3a yet avoid reaction 3b. This finding is surprising as our density functional theory (DFT) calculations for gas-phase $BR^\bullet$ radicals did not suggest that such stabilization is likely to occur, as the barrier for reaction 3b for such cations was not significantly higher than such a barrier for $BR^+$ cations that fragmented (section 3.4). Electron paramagnetic resonance (EPR) spectroscopy and pulse radiolysis are used to demonstrate that this stabilization critically involves electron delocalization over two or more cations. We suggest that $BzPy^\bullet$ and $BzPy^+$ form a dimer radical cation $(BzPy)_2^{+\bullet}$

**Received:** August 18, 2013
**Revised:** October 21, 2013
**Published:** October 22, 2013

$$BR^{\bullet} + BR^{+} \rightarrow (BR)_2^{+\bullet} \quad (4)$$

that is analogous to $\pi$-electron sandwich dimer radical cations of (neutral) aromatic molecules.[5−16] In this $(BR)_2^{+\bullet}$ dimer cation, two cofacial pyridinium rings share the excess electron. Electron-bound dimers of neutral aromatics are not very stable; however, our liquids are *ionic*, and in such solvents, reaction 4 can be stabilized by ionic interactions. We argue that stabilization via reaction 4 suppresses reaction 3b.

Even more remarkably, our results indicate that there is yet another stabilizing effect in these systems: the radiolytically produced radical dication (formed in reaction 5a) resists rapid proton loss due to the formation of a sandwich dimer involving the benzyl groups of the $BzPy^+$ cation:

$$BR^{+**} \rightarrow BR^{2+\bullet} + e^{-\bullet} \quad (5a)$$

$$BR^{2+\bullet} + BR^{+} \rightarrow (BR)_2^{3+\bullet} \quad (5b)$$

This dimer radical trication $(BR)_2^{3+\bullet}$ (paired with anions in IL), which can be viewed as a trapped-hole center, exhibits a strong charge-resonance (CR) band in the near-infrared (NIR) that is typical of other $\pi$-electron sandwich dimer cations that are well-known from previous studies.[5,6,8,12] The formation of such a highly charged species may appear counterintuitive, as there is strong Coulomb repulsion between the monomer units, but this trication can be stabilized by interactions with several anions.

Due to this charge stabilization through delocalization, a compromise between the stability of the dissociative excited states vs redox states of the cations can be reached. In the following, we substantiate these claims. EPR spectroscopy of frozen ILs and related solids is examined in section 3.1; further spectroscopic evidence is given in section 3.2 that describes pulse radiolysis kinetic studies. Section 3.3 reports product analyses of room temperature irradiated ILs using mass spectrometry and magnetic resonance techniques. Computational studies of cation dimerization are discussed in section 3.4, and conclusions are drawn in section 4.

To save space, many of the supporting tables, figures, details of synthetic and analytical protocols, and a list of abbreviations have been placed in the Supporting Information. When referenced in the text, these materials have the designator "S", as in Figure 1S.

## 2. EXPERIMENTAL AND COMPUTATIONAL METHODS

All reagents were obtained from Aldrich and used as supplied without further purification. The details of synthetic procedures (section 1S), melting points (Table 1S), nuclear magnetic resonance (NMR) spectra (section 1S and Figures 1S and 2S; see also ref 17), and mass peaks for ionic compounds (Table 2S) are given in the Supporting Information. It proved necessary to synthesize selectively deuterated isotopomers containing perdeuterated pyridine or benzyl moieties, separately and together. Such isotopomers are referred to by indicating the substitution following the moiety substituted, as in Bz-$h_7$−Py-$d_5$. *Perproteo* and *perdeutero* isotopomers of 1-ethylpyridinium (EtPy) $NTf_2$ and EtPy $PF_6$ were synthesized as described in ref 18.

Nitrogen-purged samples were placed in sealed, water-cooled, borosilicate NMR tubes (O.D. 5 mm) and irradiated by 2.5 MeV electrons to a total dose of 2.5−4.5 MGy using a dose rate of 6.8 kGy/s (1 Gy = 1 J/kg of the absorbed energy). $^1$H, $^{13}$C, $^{19}$F, and $^{31}$P NMR spectra were obtained in dimethylsulfoxide-$d_6$ (DMSO-$d_6$), using an Avance DMX 500-MHz spectrometer (Bruker); for $^1$H and $^{13}$C, the chemical shifts are given vs tetramethylsilane (TMS). $^1$H−$^1$H COSY and $^{13}$C−$^1$H HSQC two-dimensional spectroscopies were used to establish connectivity. For $^{19}$F and $^{31}$P NMR, the chemical shifts are given relative to $CFCl_3$ and $H_3PO_3$, respectively.

Tandem electrospray ionization mass spectra (ESI $MS_n$) were obtained using a Thermo Scientific LCQ Fleet ion trap mass spectrometer operating either in positive or negative modes ($MS_n^{\pm}$). $MS_1$ corresponds to the first quadrupole and $MS_2$ corresponds to collision induced dissociation (of mass selected ions) modes of operation. Liquid samples were injected directly into dilute acetonitrile solutions. $(CA)_nC^+$ and $(CA)_nA^-$ cluster ion series were typically detected, and in some cases involved product ions. In section 3.1, only $n = 0$ ions are reported.

For analysis, irradiated samples were dissolved in a minimal amount of DMSO-$d_6$ and further diluted with acetonitrile to obtain 2 wt % solutions. A 2 $\mu$L aliquot was analyzed using high-performance liquid chromatography (HPLC) (Thermo-Scientific Accela suite) with a photodiode array and ESI $MS_1^{\pm}$ detection. The chromatographic methods are summarized in Table 3S (Supporting Information). Three silica gel columns were used (separately): (i) weak cation exchange column A with carboxylate surface groups, (ii) strong anion exchange column B with $-NR_3^+Cl^-$ groups, and (iii) reverse phase column C, with the adsorbent modified by neutral aromatic groups. Liquid chromatography was used to separate and identify the products, whereas their relative yields were estimated using direct injection.

EPR experiments and DFT calculations followed the same approach as in part 1.[1] The calculations of the hyperfine coupling constants (hfcc's) and radical structures were carried out using a DFT method with the B3LYP functional[19,20] and the 6-31+G(d,p) basis set from Gaussian 03.[21] In the following, $a_{iso}$ denotes the isotropic hfcc corresponding to the hfc tensor **A** (with the anisotropic part denoted as **B**). Powder EPR spectra were simulated using first-order perturbation theory. For convenience, the principal values of the **g**-tensor are reported as $\delta g_{\nu\nu} = (g_{\nu\nu} - 2.1) \times 10^4$, where $\nu = x, y, z$ are the principal axes.

Pulse radiolysis transient absorption (TA) experiments were performed at the Brookhaven LEAF facility as previously described.[22,23] Samples were placed in 1 cm Suprasil self-masking semimicro cuvettes sealed with silicone septa and purged with argon. The doses per pulse for various experiments were 20−40 Gy. Time-resolved kinetics were obtained using FND-100Q silicon (≤1000 nm), GAP-500L InGaAs (1000−1700 nm), and GEP-600 germanium (900−1550 nm) photodiodes and digitized using Tektronix TDS-680B, LeCroy 8620A, or LeCroy WaveRunner 640Zi oscilloscopes. Interference filters were used for selection of the analyzed light. The LEAF Optical Fiber Single-Shot (OFSS) picosecond transient absorption system[23,24] was used to observe kinetics on the sub-nanosecond time scale.

1-Benzyl-3-methylpyridinium bistriflimide (Bz3MePy $NTf_2$) and 1-benzyl-4-methylpyridinium bistriflimide (Bz4MePy $NTf_2$) were kindly provided by Dr. Huimin Luo of Oak Ridge National Laboratory[25] for the pulse radiolysis studies. 1-Benzyl-3-methylimidazolium bistriflimide (BzMeIm $NTf_2$) was prepared at BNL by standard techniques by Mr. Steven Oliveri. Before the radiolysis experiments, the water content of each IL sample was confirmed to be below 100 ppm by coulometric


dx.doi.org/10.1021/jp408242b | J. Phys. Chem. B 2013, 117, 14385−14399

Karl Fischer titration. The dose per pulse was determined before each series of experiments using an $N_2O$-saturated solution of aqueous 10 mM KSCN (1 M = 1 mol/dm$^3$), where $G$ = 6.1 $(SCN)_2^-$ radicals per 100 eV absorbed and $\varepsilon$ = 7890 $M^{-1}$ $cm^{-1}$ for the $(SCN)_2^{-\bullet}$ radical at 470 nm.

## 3. RESULTS AND DISCUSSION

**3.1. EPR Spectroscopy of Frozen Samples.** Radiolysis of organic cations generally yields three types of radicals (Table 4S, Supporting Information):[26] (i) reduced ions (in our case, pyridinyl radicals; see Table 5S, Supporting Information), (ii) the corresponding proton adducts of reduced ions (at carbon-2 position) or other such adduct radicals formed when small fragment radicals or H$^\bullet$ atoms attack the aromatic rings (Table 6S, Supporting Information), and (iii) H$^\bullet$ loss radicals (Table 7S, Supporting Information). For cations with benzyl arms, elimination of the benzyl radical ($PhCH_2^\bullet$) through reaction 3b can also be expected, as discussed in the Introduction.[1,3] Using DFT simulations, we estimated hfcc's for these expected radicals, which agreed well with the experimental estimates in the literature, where available (Tables 4S−7S, Supporting Information). Figures 3S and 4S (Supporting Information) demonstrate simulated EPR spectra for these three classes of radicals (obtained using our DFT estimates). Since the deprotonation in trapped-hole species typically occurs from the loci of maximum spin density, $BzPy^{2+\bullet}$ can deprotonate from either the C(1′) or C(5′) sites. The latter reaction is more energetically prohibitive (the corresponding C−H bond dissociation energies are 4.1 eV vs 5.2 eV, respectively). The EPR spectrum for the resulting −H(5′) radical is a well-resolved triplet, whereas the −H(1′) radical appears as a doublet (Table 4S and Figure 4S, Supporting Information).

We first noticed the irregular behavior of the pyridinium cations while studying 1-*alkyl*pyridinium compounds, EtPy $NTf_2$ and EtPy $PF_6$. Assuming that pyridinium and imidazolium cations undergo similar chemistry, we expected to observe the corresponding pyridinyl radical and its proton adduct (Tables 5S and 6S, Supporting Information). Skrzypczak and Neta have suggested the formation of such pyridinyl radicals in radiolysis of neat 1-butylpyridinium tetrafluoroborate.[27] Such pyridinyl radicals can be chemically or photochemically generated in solution, and their hfcc's are well-known (Table 5S, Supporting Information). Our DFT estimates for hfcc's were in good agreement with these experimental estimates. In particular, there is $a_{iso} \sim 6.8$ G for $^{14}N$ (with $B_{||} \sim 10$ G). EPR simulations in Figure 5S (Supporting Information) indicate that EtPy-$h_{10}^\bullet$ should give a broad doublet and EtPy-$d_{10}^\bullet$ should yield a triplet of resonance lines from the $^{14}N$ nucleus (as the deuterium hfcc's are negligible). Contrary to these expectations, a narrow, structureless singlet was observed for both of the isotopomers (Figure 5S, Supporting Information). There was no indication for the formation of the pyridinyl radical, while 2-imidazolyl radicals were readily observed under the same conditions.[1,28,29]

This oddity became even more manifest for 1-benzyl derivatives. In Figure 1, we compare EPR spectra obtained in irradiated BzPy $BF_4$, BzPy $NTf_2$, and BzPy $PF_6$. It is obvious (by comparing with the EPR spectra presented in part 1) that the benzyl radical is not formed in these irradiated compounds. In BzPy Cl (Figure 6S, Supporting Information), the $Cl_2^{-\bullet}$ radical was observed, but the central line (in a dashed box) was narrow and structureless and no benzyl radical was observed. While the suppression of reaction 3b is encouraging, the progenitor BzPy$^\bullet$ radical was not observed, which reminded us of the puzzling result for $EtPy^+$ compounds.

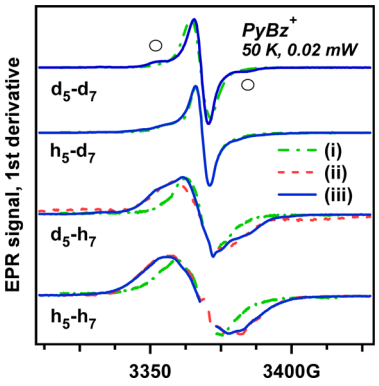


**Figure 1.** First-derivative EPR spectra for the four indicated isotopomers of 1-benzylpyridinium compounds: (i) hexafluorophosphate, (ii) tetrafluoroborate, and (iii) bistriflimide. These EPR spectra were obtained at low microwave power (0.02 mW) at 50 K. The features indicated by open circles are attributed to an anion-derived radical (see the text). See Figure 8 for interpretation of the features observed.

To provide additional insight, three isotopomers of $BzPy^+$ were synthesized. In Figure 1, we juxtaposed normalized EPR spectra obtained for irradiated $BF_4^-$, $PF_6^-$, and $NTf_2^-$ compounds of the four isotopomers. In no case did we observe the pyridinyl radical nor the expected −H(1′) and −H(5′) hydrogen loss radicals. From the comparison of the Bz-$d_7$−Py-$d_5$ and Bz-$d_7$−Py-$h_5$ isotopomers, it is seen that H/D substitution in the pyridinium moiety has a rather small effect on the overall EPR spectrum which is dominated by a single resonance line that apparently belongs to a radical derived from the benzyl moiety. At the same time, large differences are observed between the EPR spectra obtained for the benzyl-$h_7$ and benzyl-$d_7$ isotopomers with the same isotopic configuration as in the pyridinium moiety.

These observations do not exclude the formation of the pyridinyl radicals, and the Bz-$d_7$−Py-$d_5$ $NTf_2$ spectrum (Figure 1) exhibits two features (indicated by open circles in the plot) that can be taken for M($^{14}$N) = ±1 lines of Bz-$d_7$−Py-$d_5^\bullet$ (cf. the simulations in Figure 3S, Supporting Information). When the sample temperature was increased over 150 K, the organic radicals decayed and another radical was observed (Figure 7S, Supporting Information). EPR spectra of this radical are similar for $h_7$−$h_5$ and $h_7$−$d_5$ and $d_7$−$h_5$ and $d_7$−$d_5$ isotopomers, respectively (Figures 8S and 9S, Supporting Information), and this species was also observed in some other bistriflimide systems. This is a protonated radical that is derived from $NTf_2^-$ with $\delta g$ = (108, 45, 0) and $A_z(^1H) \sim 20$ G that we attribute to $^\bullet SO_2NHTf$ (the protonated residue of trifluoromethyl elimination). Resonance lines that can be potentially attributed to BzPy$^\bullet$ in Figure 1 are, in fact, from this anion-derived radical, and these resonance lines are not observed in the hexafluorophosphate system (Figure 2). We conclude that electron localization in $BzPy^+$ compounds does not yield pyridinyl nor benzyl radicals.

In the imidazolium compounds, electron scavenging by the parent cation can be suppressed by a protic impurity and/or electron-accepting anions. Electron irradiation of HPy $BF_4$ (pyridinium tetrafluoroborate, not shown) yields M($2^1$H) = ±1 lines corresponding to two equivalent protons with 69 G coupling that is consistent with the H atom adduct of the


dx.doi.org/10.1021/jp408242b | J. Phys. Chem. B 2013, 117, 14385−14399

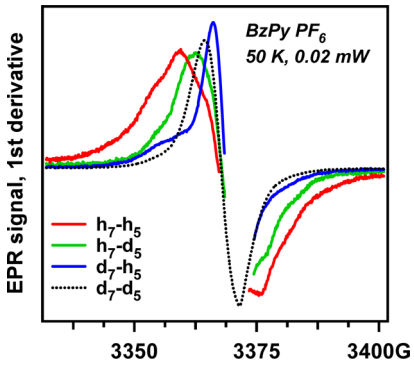


**Figure 2.** First-derivative, low-power EPR spectra for the four isotopomers of 1-benzylpyridinium hexafluorophosphate as indicated in the plot. These EPR spectra have been scaled and overlapped for the convenience of comparison.

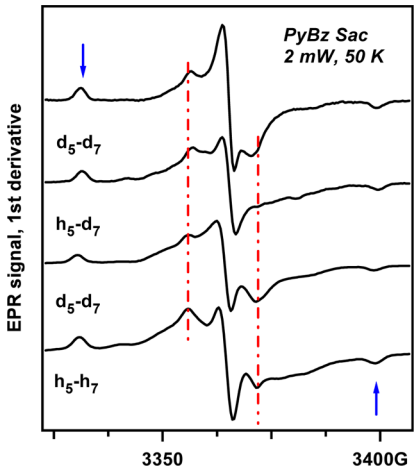


**Figure 3.** Like Figure 2, for the four isotopomers of 1-benzylpyridinium saccharinate, as indicated in the plot. The vertical lines and arrows indicate the resonances from the imidyl radical that can be contrasted by isothermal annealing (see Figure 11S, Supporting Information). Trapping of electron as the >NH$^{-\bullet}$ radical does not occur in the 1-benzylpyridinium saccharinate.

parent cation (Tables 4S and 6S, Supporting Information). The outer M($2^1$H) = ±1 lines corresponding to a hfcc of 40−50 G (Table 6S, Supporting Information) are observed for Bz-$h_7$−Py-$h_5$ $BF_4$ warmed to 300 K (Figure 10S, Supporting Information). For the Bz-$h_7$−Py-$d_5$ cation, the H adduct should appear as a doublet if the H atom attaches to the pyridinium ring and a triplet if it attaches to the benzyl ring (Table 6S and Figure 4S, Supporting Information). Our results suggest that both modes of H atom attachment occur in irradiated Bz-$h_7$−Py-$d_5$ $BF_4$:$H_3O^+$ (Figure 10S, Supporting Information). At 50 K, there are two lines separated by 90 G, which originate from a triplet, which would arise if the H atom attaches to the phenyl-$h_5$ ring. When the sample is warmed to 225 K, there is a M($^1$H) = ±1/2 doublet with a coupling constant of 67 G and the additional hyperfine structure due to coupling to a single $^{14}$N nucleus. The latter feature would originate from the H atom adduct at carbon-2 of the pyridinium moiety (Figure 10S and Table 6S, Supporting Information): one of the H adducts is more stable than the other one at a higher temperature. We conclude that H atoms generated by electron scavenging via the $H_3O^+$ impurity can attach to both aromatic rings of the $BzPy^+$ cation. More importantly, it is seen that the yield of such H adducts is relatively low and the same resonance lines that are observed in Figures 1 and 2 also occur in the tetrafluoroborate systems. Thus, in BzPy $BF_4$:$H_3O^+$, only some electrons are scavenged by the protic impurity, whereas, in the corresponding 1-benzyl-3-methylimidazolium ($BzMeIm^+$) system, *all* of the electrons were scavenged by this impurity. This indicates that, in the frozen glassy IL, *$BzPy^+$ cations scavenge electrons more efficiently than $BzMeIm^+$ cations and about as efficiently as hydronium ions.*

Just how deeply the electron is trapped by the $BzPy^+$ cations is indicated by the EPR spectra shown in Figure 3. In BzMeIm Sac (Figure 3 in part 1),[1] both electrons and holes are scavenged by the *anion*, so there is little difference between the $h_7$ and $d_7$ isotopomers on $BzMeIm^+$ and there is a strong resonance line from the >NH$^{-\bullet}$ radical (the protonated electron adduct). The latter contribution is not observed for BzPy Sac at all (Figure 3), and there is significant isotope variation of the observed EPR spectra. When the samples are isothermally annealed at 77 K, trapped-hole centers (>N$^\bullet$ radicals) abstract H atoms from organic ions in the matrix, so it is possible to isolate the contribution from this imidyl radical, as done in Figure 11S (Supporting Information). The corresponding difference traces exactly correspond to the >N$^\bullet$ radicals as observed in irradiated K Sac.[18] We conclude that, in BzPy Sac, the saccharinate anion scavenges only holes, while, in BzMeIm Sac, it scavenges both electrons *and* holes. It is seen that $BzPy^+$ cations trap electrons so strongly that these cations can compete with hydronium and outcompete the saccharinate anions.

It is clear from these experiments that electron localization in pyridinium ILs does not follow the pattern observed for ILs composed of cations derived from five-atom heterocycles.[1]

**3.2. Pulse Radiolysis.** After the ionization event and subsequent relaxation steps, excess electrons in ILs occur in two general forms: (i) "solvated electrons" (presumably, cavity-type F-center defects, where the electron occupies a void stabilized by Coulomb interaction with several cations)[30−32] and (ii) localized states, such as neutral radicals (if the excess electron occupies the lowest unoccupied orbital of a single cation) or radical cations (if the electron is shared by two or more cations).[26,33] In ILs with aliphatic cations, the excess electrons may persist for up to a few microseconds as "solvated electrons"[34−37] (except in cases where they react with the constituent anion).[17]

In aromatic ILs, the mode for electron localization is not as clear and may be more variable. Originally, it was assumed that such systems localize electrons on a single cation to form a neutral heteroaromatic radical, as they do when these cations are dissolved in water.[38−40] In contrast, dynamic *ab initio* simulations of excess electrons in neat imidazolium and pyridinium chloride ionic liquids by Wang et al.[41,42] have predicted sharing of electron density by $\pi^*$ orbitals of several aromatic cations, including delocalized states in dynamic equilibrium with states associated with only one or two cations, with the occupancy of the various states varying with liquid fluctuations. However, it must be kept in mind that the simulations were performed at theoretical temperatures of 425−440 K, so the populations of various states may be different at lower temperatures (e.g., room temperature or frozen glasses at 77 K) or in the presence of anions other than chloride (which can donate electron density to the cation through H-bonding). It is also important to remember that the solvation dynamics of ILs extend into time scales of hundreds


dx.doi.org/10.1021/jp408242b | J. Phys. Chem. B 2013, 117, 14385−14399

to thousands of picoseconds,[43] even for excess electrons.[23] Therefore, the predictions of 3−7 ps trajectories could be valid on that time scale, but they are not necessarily reflective of the fully relaxed systems.[32,44]

EPR results for 1-alkylimidazolium systems are consistent with the strongly localized states owing to their stabilization by pyramidal distortion at the $C_2$ position, often followed by subsequent reactivity;[1,29,33] however, similar relaxation is not available to electron adducts of the pyridinium systems.

Given how deeply the electron is trapped in the 1-benzylimidazolium cations in the corresponding ILs,[1,26,29,33] on the time scale pertinent to our observations, the trapped-electron center is almost certainly a localized state. Furthermore, since (as will be shown elsewhere) in dilute solution $BzPy^+$ irreversibly scavenges "solvated electrons" in aliphatic ILs, such as 1-butyl-1-methylpyrrolidinium bistriflimide ($C_4$mpyrr $NTf_2$, $k = 5.3 \times 10^8$ $M^{-1}$ $s^{-1}$),[45] it is unlikely that the postulated coexistence of delocalized and localized states occurs. Regardless, the simulations of Wang et al.[42] indicate multiple modes of electron localization for pyridinium ions. As shown in section 3.1, EPR spectroscopy indicates that 1-alkylpyridinium and 1-benzylpyridinium cations localize electrons in a different fashion than the corresponding imidazolium cations. To obtain further insight, we complement our EPR results by pulse radiolysis−transient optical absorption spectroscopy.

Figure 4 shows the transient spectra of several $NTf_2$ ionic liquids containing benzyl functionalities and others with simple

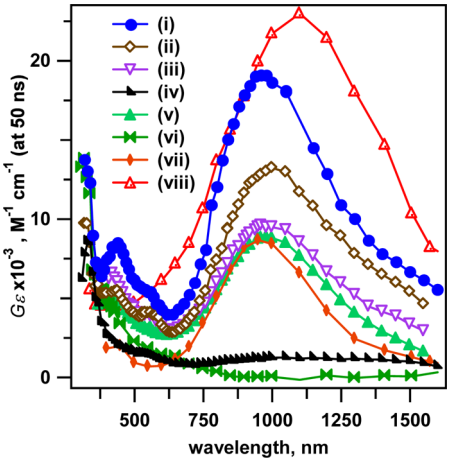


**Figure 4.** Pulse radiolysis transient absorption spectra for eight bistriflimide ILs, derived from integrated time slices between 50 and 55 ns after the electron pulse. They are scaled as the product of the radiolytic yield $G$ (in species per 100 eV) and the extinction coefficient $\varepsilon$ (in $M^{-1}$ $cm^{-1}$), based on thiocyanate dosimetry. The cation partners of $NTf_2^-$ anion are (i) 1-benzylpyridinium, (ii) 1-benzyl-3-methylpyridinium, (iii) 1-benzyl-4-methylpyridinium, (iv) 1-butylpyridinium, (v) 1-benzyl-3-methylimidazolium, (vi) 1-ethyl-3-methylimidazolium, (vii) 1-benzyl-1-methylpyrrolidinium, and (viii) 1-butyl-1-methylpyrrolidinium. Data for (vi) were rescaled from ref 29. The lines connecting symbols are guides to the eye.

alkyl groups for comparison. The spectra in Figure 4 represent integrated time slices between 50 and 55 ns after the electron pulse, and they are scaled as the product of the radiolytic yield $G$ (in molecules per 100 eV absorbed) and the extinction coefficient $\varepsilon$ (in $M^{-1}$ $cm^{-1}$), based on thiocyanate dosimetry as described in section 2. Thus, they are all normalized to the same radiolytic dose, and their intensities can be compared. The observed spectra clearly represent the sum of multiple transient species, whose dynamics and reactivity will be the subject of another report.

Before examining the transient absorption of irradiated benzyl-containing ILs, it is useful to examine the spectra of ILs with simple alkyl groups. The strong and very wide absorption band in $C_4$mpyrr $NTf_2$ is due to the aforementioned solvated electron.[23,35,37] The 50 ns transient spectrum of 1-ethyl-3-methylimidazolium bistriflimide (EtMeIm $NTf_2$), reproduced here (scaled for dose) from ref 29, shows very low absorbance to the red side of 800 nm. Our spectrum of neat 1-butylpyridinium bistriflimide (BuPy $NTf_2$) agrees with that reported between 290 and 450 nm by Behar et al.;[40] here, it has been extended to the near-infrared (NIR) where there is a very broad but relatively weak absorption band in addition to the features previously seen in the ultraviolet and visible. Either there is a dynamic equilibrium between the localized and solvated electron states (with a minority population of the latter states contributing to the NIR band) or this absorption band arises from a localized state. Since the pyridinyl radical does not absorb in the NIR, it cannot be the origin. Given the insights of Wang et al.,[41,42] the observed broad and weak NIR absorption could be interpreted as charge resonance (CR) band(s) arising from the excess electron shared by two or several cations. Since the interaction between the two units is weak (the distance is >3.5 Å and the binding energies are 0.5−0.8 eV),[7,14,15] the bands are observed in the NIR.

All of the ILs containing benzyl-derivatized cations $BzC^+$ (C = pyridinium, imidazolium, and pyrrolidinium) show strong and broad absorption features peaking between 960 and 1000 nm and tailing into the NIR. We attribute these absorption bands to CR states where an excess charge (electron or hole) is stabilized by delocalization over two (or more) aromatic moieties (including both the benzyl groups and the aromatic cations). The most common type of CR state is the aromatic radical dimer cation, which is formed by the attachment of a hole to two aromatic molecules. The CR band arises from excitation from the symmetric doubly occupied highest occupied molecular orbital of the dimer to the antisymmetric singly occupied molecular orbital.[6,14] A pertinent example is the benzene dimer radical cation $(C_6H_6)_2^+$, whose CR absorbance band peaks around 920 nm in neat benzene[8] and at 880 nm in 2-methylpentane at 82 K.[12] The benzene trimer radical cation $(C_6H_6)_3^+$ was also observed in the latter study with an absorption peak at 1380 nm. In the case of the benzyl-derivatized ILs, similar CR states can be formed when two benzyl groups associate to delocalize a hole (reactions 5a and 5b) to produce a dimer radical trication $(BzPy)_2^{3+\bullet}$ that is stabilized by the anions of the surrounding matrix.

The case for hole-centered CR states in irradiated benzyl ILs is strong, but the contribution of electron-centered CR states to the observed NIR spectra should not be ignored. CR absorptions in such systems arise from electronic transitions from the singly occupied to the lowest unoccupied molecular orbital. Aromatic dimer radical anions are much less common than cations but several reports exist, and the group of Majima has documented two pertinent examples. The first[16] is a series of cyclophanes where two aryl groups are constrained into a face-to-face orientation to varying degrees by the number and location of linking groups. Upon addition of an electron, the anionic CR states have absorption bands in the same region as we observe in Figure 4 ($\lambda_{max}$ = 800−1200 nm). The


dx.doi.org/10.1021/jp408242b | J. Phys. Chem. B 2013, 117, 14385−14399

constrained geometries of the cyclophanes result in narrower bands, but the ensemble of the various cyclophanes mimics what might be observed by the conformational distribution of aryl moieties in the unconstrained ionic liquid.

The second example[46] is a selection of anions formed from polyphenylalkanes containing 1,1-diphenylmethyl groups. (This 1,1-diphenylmethyl motif is isostructural and isoelectronic with the $BzPy^+$ cation.) In these systems, the excess electron was found to be delocalized over two geminate phenyl groups having an edge-to-face configuration in preference to all other available interactions. An examination of the concentration independence of the radical anion absorption spectra confirmed that this interaction was intramolecular. The CR bands for this series lie to the red of the ones we observe in Figure 4 ($\lambda_{max}$ = 1210−1830 nm); however, it is possible that environmental factors in the ILs could shift the energy of this band. Nevertheless, in spite of the structural and electronic similarities of the 1,1-diphenylmethyl motif to 1-benzylpyridinium cations, the intramolecular CR interaction does not seem to operate for excess electrons in ILs containing the $BzPy^+$ cation, since the solvated electron absorbance at 900 nm in $C_4$mpyrr $NTf_2$ decays to zero in the presence of 21−52 mM BzPy $NTf_2$ instead of producing the CR absorption seen in Figure 4 (also see Figure 12S, Supporting Information).

The question arises whether the observed transient absorption bands in the benzyl-derivatized ILs originate from electron- or hole-derived CR states. To address this question, we added electron and hole "scavengers" (saturated $N_2O$ and 0.4 M $NEt_3$, respectively) to BzPy $NTf_2$ and observed the change in decay kinetics of the CR absorption in the NIR, as shown in Figure 5. (The solubility of $N_2O$ in BzPy $NTf_2$ is unknown, but the solubility of $CO_2$ in the same IL is 75 mM[25] and the solubilities of both gases in ILs tend to be similar.[47−50]) Addition of either scavenger causes the CR absorption at 900 nm to decay at accelerated rates compared to the neat, argon-saturated IL. Very similar results were obtained in 1-benzyl-1-methylpyrrolidinium bistriflimide at 850 nm. We therefore conclude that both electron- and hole-derived CR states contribute to the observed absorption bands. The spectroscopy and reactivity of both CR states in benzyl-derivatized ILs will be the subject of further studies.

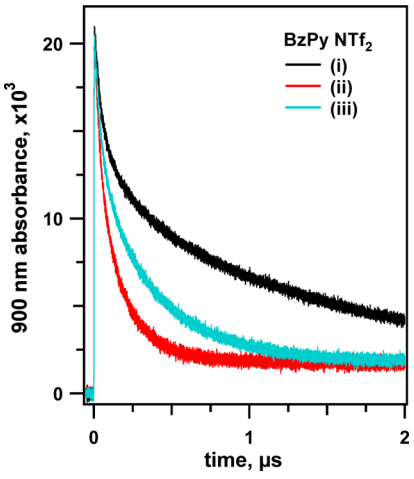


**Figure 5.** Pulse radiolysis transient absorption kinetics measured at 900 nm. Three samples were examined: neat BzPy $NTf_2$ saturated with argon (i) or $N_2O$ (ii) and an argon-saturated solution of 0.4 M triethylamine in BzPy $NTf_2$ (iii).

Picosecond pulse radiolysis measurements were made using the BNL OFSS TA system[24] to probe the early time (<5 ns) reactivity and dynamics of the observed transient species. The same BzPy $NTf_2$ samples with and without scavengers used in Figure 5 were examined at five wavelengths between 750 and 900 nm, and the results are shown in Figure 13S (Supporting Information). Figure 13S(a) (Supporting Information) shows that on the 5 ns time scale there is no difference in the transient absorption signals at 900 nm in the presence of scavengers or not. This was true at all five of the wavelengths measured. Unlike the case of the solvated electron in aliphatic ILs where scavenging of presolvated electron states reduces the early time absorbance,[23,34,36] in BzPy $NTf_2$, the scavengers cannot compete with the large concentration of preformed charge traps formed by the close association of arene functionalities in the IL. The spatial distributions of the benzyl groups, pyridinium (or other) cations, and the anions within the IL play a role in the trapping and stabilization of excess charges in CR states.

The importance of this "tertiary IL structure" in CR state stabilization is suggested by comparison of the NIR spectra of BzPy $NTf_2$ and BuPy $NTf_2$ in Figure 4. The CR absorption observed between 800 and 1600 nm in BuPy $NTf_2$, presumably due to $(BuPy)_2^{+\bullet}$ dimer cations formed by electrons interacting with two pyridinium cations, is much weaker than the absorbance of BzPy $NTf_2$ (although hole CR states also contribute in this case). This could be due to a lower absorptivity or equilibrium quotient for formation and/or weaker interactions, as suggested above, both of which could be affected by the tertiary structure of the BuPy $NTf_2$ IL, which lacks aryl groups and thus would be organized in a different way (e.g., the structure of 1-hexylpyridinium bistriflimide,[51] where the pyridinium rings do not directly interact). Scattering techniques and molecular dynamics simulations[52] will be used to resolve the structures of these ILs and their effects on excess charge reactivity.

Figure 13S(b) (Supporting Information) shows the OFSS TA traces in BzPy $NTf_2$ for all the wavelengths measured. It is clear by comparison of the various wavelengths that multiple species contribute to the observed absorption signals. It is interesting to note the ~500 ps time constant of the 25% rise in absorbance at 900 nm. BzPy $NTf_2$ has a viscosity of 197 cP at 20 °C, and considering the electron solvation time for solvated electrons in $C_4$mpyrr $NTf_2$ (that has a viscosity of 95 cP) is ~270 ps,[23] the 500 ps rise time is on the order of the expected average solvation time in this IL. This means that the observed absorbance change could be related to dynamical relaxation upon addition of an excess charge, stabilizing the CR state and blue-shifting its absorption. The resolution of the individual spectral contributions and their relaxation dynamics will be explored further after the addition of NIR cameras to the OFSS system, which is in progress.

From the point of view of radiation stability, the attractive feature of the 1-benzylpyridinium system is that it yields *π-electron sandwich dimers both in electron and hole localization; this dimerization significantly reduces the efficiency of reaction 3b and deprotonation, respectively.*

**3.3. Product Analyses.** While these spectroscopic results suggest the increased radiolytic stability of 1-benzylpyridinium cations, it remains to be seen whether these properties translate into decreased degradation during continuous irradiation. To


dx.doi.org/10.1021/jp408242b | J. Phys. Chem. B 2013, 117, 14385−14399

Table 1. Mass Peaks of Product Cations in Irradiated 1-Benzylpyridinium Bistriflimide (BzPy $NTf_2$, 3.05 MGy)

| | +m/z | | | | | isotopic mass shift | | | |
|---|---|---|---|---|---|---|---|---|---|
| attribution | $h_5-h_7$ | $d_5-h_7$ | $h_5-d_7$ | $d_5-d_7$ | fragment | $d_5-h_7$ | $h_5-d_7$ | $d_5-d_7$ | area % |
| $PhCHF^{+}$ [a,b] | 109.1 | 109.1 | 115.2 | 115.2 | F | 0 | 6 | 6 | 2.2 |
| $PhCHCF_3^{+}$ [a,b] | 159.3 | 159.3 | 165.2 | 165.2 | | 0 | 6 | 6 | 0.5 |
| $BzPy^{+}$ [a,b,c,d] | 170.2 | 175.2 | 177.2 | 182.3 | Py | 5 | 7 | 12 | 100 |
| $BzPy-F^{+}$ * [b,c] | 188.1 | 193.2 | 194.2 | 199.3 | Py | 5 | 6 | 11 | 3.3 |
| $BzPy-CF_3^{+}$ * [a,b] | 238.1 | 243.2 | 244.3 | 249.3 | Py | 5 | 6 | 11 | 23.0 |
| $BzPy-Py^{+}$ * [a,b] | 247.2 | 256.3 | 259.3 | 264.3 | Py | 9 | 6 | 15 | 1.3 |
| $BzPy-Bz^{+}$ * [b] | 260.2 | 264.3 | 273.3 | 278.4 | Py | 5 | 13 | 18 | 3.0 |
| $BzPy-C_2F_5^{+}$ * [a,b] | 288.2 | 293.2 | 294.2 | 299.3 | | 5 | 6 | 11 | 1.7 |
| $BzPy-CF_3-CF_3^{+}$ * [a,b] | 306.7 | 311.3 | 311.4 | 316.7 | Py | 5 | 5 | 10 | 1.9 |
| $BzPy-HNTf^{+}$ * [a,b,c] | 317.2 | 322.2 | 323.4 | 329.3 | Py | 5 | 6 | 12 | 1.3 |
| $BzPy-Bz-CF_3^{+}$ * [a,b] | 328.2 | 333.3 | 340.3 | 345.8 | | 5 | 12 | 17 | 1.1 |
| $BzPy-SO_2NHTf^{+}$ * [c] | 381.2 | 386.3 | 387.3 | 392.0 | | 5 | 6 | 11 | |
| $BzPy-CF_3NTf^{+}$ * [a,b,c] | 385.2 | 390.2 | 391.3 | 396.3 | Tf | 5 | 6 (5)[b] | 11 (10)[b] | 1.0 |
| $Bzpy-CF_2SO_2HNTf^{+}$ * [b,c,e] | 431.2 | 436.2 | 437.2 | 442.2 | | 5 | 6 | 11 | |

[a−c]Observed in LCMS. The symbols correspond to columns/methods a−c in Table 3S (Supporting Information). [d]Parent ion, scaled to 100. [e]Not observed in direct sample injection.

this end, we irradiated bistriflimide, hexafluorophosphate, and saccharinate salts of 1-benzylpyridinium, using selective isotope substitution in order to make inferences concerning the product structure. High dose and high dose rate conditions were used. In industrial nuclear separations, the total dose per solvent use cycle is ∼0.5 MGy (vs 2.5−4.5 MGy in our experiments),[53] and the dose rate is over $10^3$ times lower than in our electron beam experiments. Since the yield of cross recombination depends on the steady-state concentration of radiolytically generated radicals, these high dose rate conditions represent the worst-case scenario. If the material is stable to radiolytic decomposition under such harsh conditions, this is a strong indication that it is also suitable under realistic irradiation conditions.

Another rationale for using such punishing regimens is the very success of our approach: product yields were so low that the product concentrations were often lower than those of impurities originally present in the sample. Since there were many such low-yield products, their mass peaks were closely spaced, and this complicated their attribution due to the occurrence of isobaric resonances. For that reason, chromatographic separation was used (section 2). While no HPLC column fully separated all of the products, the latter were separated into several groups with similar retention times, and isobaric products typically belonged to different groups. This approach allowed us to accurately determine isotope shifts for each product identified in the reaction mixture. The relative yields of these mass peaks were determined by direct ESI $MS_1$ spectrometry; in this way, the data presented in Tables 1−3 and 8S−13S (Supporting Information) were generated. Further structural inferences were obtained using NMR spectroscopy methods, as explained below.

We begin with Tables 1 and 2 for radiolysis of BzPy $NTf_2$. The main cation product of this radiolysis is the trifluoromethyl radical adduct of the parent cation (Table 1). As seen from Table 1, $d_5$-substitution in the pyridinium group of the parent $BzPy^{+}$ cation changes the mass of this product by 5 amu, whereas $d_7$-substitution in the benzyl group changes it by 6 amu. This indicates that the $CF_3^{\bullet}$ radical attaches to the benzyl group. Similar mass shift analyses for other products indicate that *all* of the products with masses greater than $BzPy^{+}$ are

Table 2. Mass Peaks of Product Anions in Irradiated 1-Benzylpyridinium Bistriflimide (BzPy $NTf_2$, 3.05 MGy)

| attribution | −m/z | fragment | area (%) |
|---|---|---|---|
| $NSO_2F^{-}$ | 97 | F | 0.08 |
| $NTf^{-}$ | 147 | $SO_2$ | 1.8 |
| $TfO^{-}$ | 148 | | |
| $SONTf^{-}$ | 195.4 | $CF_3$ | 0.1 |
| $SO_2NTf^{-}$ | 211 | $SO_2$ | 0.2 |
| $CF_3NTf^{-}$ | 216.4 | $CF_3$ | 0.3 |
| $FSO_2NTf^{-}$ | 230 | | 1.2 |
| $CF_3SONTf^{-}$ | 264.3 | $CF_3$ | 0.2 |
| $NTf_2^{-}$ [a] | 280 | | 100 |
| $C_2F_5SO_2NTf^{-}$ | 330.2 | | 0.2 |
| $NTf_2-CF_2SO_2^{-}$ | 411.2 | | 0.2 |

[a]Parent ion, scaled to 100%.

derived either from fragments of the parent cation (pyridine and benzyl) or anion (such as $-CF_3$, $-SO_2NTf$, $-NTf$, and $-CF_2SO_2NTf$) that are *attached to the benzyl group of the parent cation* (such products are indicated by an asterisk in Tables 1 and 3). Our EPR studies[28,29] as well as product analysis by Moisy and co-workers[54−56] suggest that bistriflimide readily fragments in radiolysis; the loss of fluoride and trifluoromethyl are the main two channels for anion decomposition. In accordance with these results, $BzPy-CF_3^{+}$ is the main radiolytic product, but the high yield of the $^{\bullet}CF_3$ radical also causes its addition even to other *adducts*. The significant extent of fragmentation in the bistriflimide ion can be observed from the multiple fragment (Table 2) and combination (Table 1) ions. Several of the cation products are $BzPy^{+}$ modified by (protonated) anions from Table 2. It is possible that such species can also exist in deprotonated (zwitterion) states that escape observation by ESI $MS_1$; however, with the single exception of the $BzPy-CF_2SO_2NHTf^{+}$ adduct (Table 1), the same mass peaks were observed in solutions containing 0.1 wt % formic acid; i.e., the radiolyzate was sufficiently acidic to shift the protonation equilibria to the cation side.

Most remarkable is the complete absence of $HPy^{+}$ cations, suggesting a low yield of fragmentation in the parent $BzPy^{+}$ cation. The elimination of the benzyl group certainly occurs, as


dx.doi.org/10.1021/jp408242b | J. Phys. Chem. B 2013, 117, 14385−14399

Table 3. Mass Peaks of Product Cations in Irradiated 1-Benzylpyridinium Hexafluorophosphate (BzPy $PF_6$, 3.3 MGy)

| | +m/z | | | | | isotopic mass shift | | | |
|---|---|---|---|---|---|---|---|---|---|
| attribution | $h_5-h_7$ | $d_5-h_7$ | $h_5-d_7$ | $d_5-d_7$ | fragment | $d_5-h_7$ | $h_5-d_7$ | $d_5-d_7$ | area % |
| $PhCHF^{+}$ [a,b] | 109.1 | 109.1 | 115.2 | 115.2 | F | 0 | 6 | 6 | 0.23 |
| $BzPy^{+}$ [a,b,c,d] | 170.2 | 175.2 | 177.2 | 182.2 | Py | 5 | 7 | 12 | 100 |
| $BzPy-F^{+}$ * [a,c] | 188.2 | 193.2 | 195.3 | 199.3 | Py | 5 | 7 | 11 | 0.94 |
| $BzPy-Py^{+}$ [a,b] | 247.2 | 256.2 | 253.3 | 262.3 | Py | 9 | 6 | 15 | 1.00 |
| $BzPy-Bz^{+}$ * [a,b] | 260.3 | 265.3 | 273.3 | 278.3 | Py | 5 | 13 | 18 | 3.60 |
| $BzPy-HPF_4^{+}$ * | 278.2 | 283.2 | 285.3 | 289.3 | | 5 | 7 | 12 | 1.70 |
| $BzPy-Py-Bz^{+}$ [a,b,c] | 337.4 | 346.4 | 349.3 | 358.6 | | 9 | 12 | 21 | 0.43 |

[a−c]Observed in LCMS. The symbols correspond to columns/methods a−c in Table 3S (Supporting Information). [d]Parent ion, scaled to 100%.

there are products of recombination of this species with F and $CF_3$, and there are also pyridine and benzyl adducts of the $BzPy^{+}$ cation. However, the corresponding yields are quite low. The yields of BzF and $BzCF_3$ are 2 and 0.5%, respectively, and the yields of the Py and Bz adducts of $BzPy^{+}$ are 1.3 and 3%, respectively (where 1% corresponds to the *G*-value of 0.07 species per 100 eV absorbed). In contrast, the yield of the trifluoromethyl adduct corresponds to 1.6 species per 100 eV.

Thus, in BzPy $NTf_2$, the cation fragmentation is suppressed to an extent that is negligible as compared to modification of the parent cations by fragments of anion decomposition: *the overall radiation stability is defined by anion rather than cation stability*. The latter is poor: the $^{19}F$ NMR spectrum (see Table 14S, Supporting Information) indicates 30+ groups of (mainly singlet) resonance lines from the products that integrate to 1.32 $^{19}F$ nuclei. Two trace products (<0.3% yield) with a chemical shift of −124 ppm exhibit proton couplings of ∼54 Hz that are typical of F-atom substitution at carbon-1′. This indicates that fluorination mainly occurs in the phenyl ring. The latter is also suggested by a group of products with chemical shifts of −112 to −116 ppm that are coupled to several aromatic protons (see Table 14S, Supporting Information). The three main products (integrating to >1% yield) have chemical shifts around −78 or −61 ppm. The resonance lines correspond to proton-decoupled $CF_3$ groups, which is consistent with our interpretation of mass spectra given in Table 1.

Further inferences can be obtained from $^{1}H$ and $^{13}C$ NMR spectra (Figures 14S and 15S, respectively, Supporting Information). Using $^{1}H-^{1}H$ and $^{1}H-^{13}C$ two-dimensional correlation spectroscopies, it is possible to divide the many resonance lines from the products observed in the $^{1}H$ NMR spectrum into several proton connectivity groups belonging to different products (Figure 14S, Supporting Information). The main product (group A) has resonance lines at 8.71 (d, 2), 8.21 (t, 4), and 7.75 (t, 3) ppm that can be compared to, respectively, 9.19 (d, 2), 8.64 (t, 4), and 8.19 (t, 3) ppm in the pyridinium group (following the atom numeration of Scheme 1). Upon the addition of 1 M $d_4$-acetic acid, the chemical shifts in this product change to 8.79, 8.31, and 7.83 ppm, suggesting that this product cannot be pyridine, which would be completely protonated under such conditions (the chemical shifts for pyridine and pyridinium in DMSO-$d_6$ are 8.60, 7.74, and 7.35 ppm and 8.90, 8.61, and 8.07 ppm, respectively). Carbon-13 shifts (in ppm, Figure 15S, Supporting Information) for this product are 145.2 (4), 141.7 (2), 125.6 (3), and 62.7 (1′) vs 145.9, 144.5, 128.4, and 63.5, respectively, in the parent cation; the former resonance lines certainly originate from a pyridinium group; the bridging carbon-1′ is not coupled to fluorine-19. The second largest group of resonance lines has chemical shifts at 8.99 (d, 2), 8.15 (t, 4), and 7.27 (t, 3); once again, these shifts correspond to an intact pyridinium group. Other groups of resonance lines are also inconsistent with either pyridine or $HPy^{+}$ present in the reaction mixture; in fact, all of these groups can be accounted for as modifications in the benzyl arm of the cation, in agreement with our earlier conclusion. Even if pyridine is released, it becomes attached to the parent cation.

Scheme 1. Structural Formulas for 1-Benzyl-4-X-pyridinium ($Bz4XPy^{+}$, Where X = H, Me, or NC) Cations and Saccharinate ($Sac^{-}$) and Bistriflimide ($NTf_2^{-}$) Anions

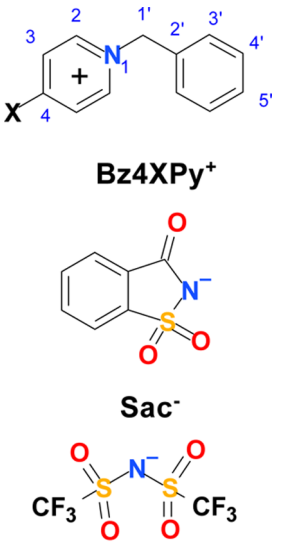


From these MS and NMR results, it follows that in BzPy $NTf_2$ the anion is so much more unstable than the cation that the fragmentation of the latter hardly matters at all. Hexafluorophosphate is more radiation stable than bistriflimide,[1,54,56] so it offers a better way to evaluate *cation* stability. The $^{19}F$ NMR spectrum of irradiated BzPy $PF_6$ (Table 15S, Supporting Information) reveals two doublets at −72.3 ppm ($J(^{19}F-^{31}P)$ = 916.6 Hz) and −78.98 ppm ($J(^{19}F-^{31}P)$ = 951.7 Hz) that have their complements in the $^{31}P$ NMR spectrum at −144.2 (m), −7.62 (d), and −15.7 (t) ppm. These products contain a single $^{31}P$ nucleus and, respectively, one or two $^{19}F$ nuclei. The −79 ppm ($^{19}F$) product is the strongest resonance (integrating to 0.17 $^{19}F$), and the second strongest resonance is at −166.5 ppm (a singlet integrating to 0.154 $^{19}F$). In total, all F-containing products integrate to 0.42 $^{19}F$. Most of these products (Table 15S, Supporting Information) have chemical shifts between −59 and −49 ppm, and many of them are


dx.doi.org/10.1021/jp408242b | J. Phys. Chem. B 2013, 117, 14385−14399

coupled to the $^{31}P$ nucleus (with $J(^{19}F-^{31}P)$ of 800−970 Hz) or a spin-1/2 nucleus other than the proton (with $J(^{19}F-X)$ of ∼45 Hz). In the $MS_1^+$ spectra, there is a peak corresponding to $PO_2F_2^-$, which is the product of $PF_6^-$ hydrolysis, and it appears that this anion and $PO_3F^{2-}$ (which is the product of its further hydrolysis) are the main products of radiolysis. This hydrolysis occurred by a reaction of an identified precursor with traces of water present in organic solvents used to analyze the samples. There is no indication for extensive modification of the cation by $^{19}F$-containing fragments.

These results are corroborated by the data in Table 3. There are Bz−F and BzPy−F substitutions, as in BzPy $NTf_2$, and there are Py- and Bz-substitutions corresponding to 1 and 3.6% modification of $BzPy^+$. There is also $-PF_4$ substitution in the benzyl ring (1.7%) and a C−C bridged dimer cation (0.4%). In the $^1H$ NMR (Figure 16S, Supporting Information), there are three lines from the protons in the pyridinium headgroup (8.86, 8.52, and 8.01 ppm) having complementary $^{13}C$ shifts of 114.9, 142.9, and 126.7 ppm, respectively (Figure 17S, Supporting Information). Once again, modification of the $BzPy^+$ cation is the predominant degradation pathway; the fragmentation yield is negligibly small.

In section 3.1, we observed that, in the saccharinate systems, radical (ions) originated mainly from the anion. In the $MS_1^-$ spectra of irradiated BzPy Sac (Table 9S, Supporting Information), there is a C−C dimer saccharinate anion that was also observed in other saccharinate systems;[18] this species is likely to occur through radical addition to the parent anion. In the $MS_1^+$ spectra, there are cation adducts of the benzyl and saccharinate that are present in substantial yield (7−8%). Two groups of modified $BzPy^+$ cations are also suggested by $^1H$ NMR spectra (Figure 18S, Supporting Information). Therefore, radiolytic "protection" of the anion against fragmentation[18,57−59] comes at a price, as this anion yields reactive radicals that attach to $BzPy^+$ cation.

In section 3.2, we speculated that the increased stability of 1-benzylpyridinium cations is due to its collective modes for charge delocalization. Since the $BzPy^+$ cation is too hydrophilic for practical use in extractions from water, it is important to assess how derivatization of this cation affects its radiation stability. To this end, we investigated 4-methyl and 4-cyano derivatives of 1-benzylpyridinium bistriflimide and hexafluorophosphate. These two modifications represent the inclusion of electron donating and withdrawing groups, respectively, charting the two extremes. The EPR spectrum for irradiated Bz4MePy $NTf_2$ yields a featureless, narrow Gaussian line that does not correspond to H loss and pyridinyl radicals (Figure 19S, Supporting Information). Thus, at this qualitative level, the mode of electron localization in 4-methyl and 3-methyl derivatives is similar to the $BzPy^+$ cation, as suggested by the pulse radiolysis results.

As seen from Table 10S (Supporting Information) for Bz4MePy $NTf_2$, the radiolytic products are remarkably similar to those observed in BzPy $NTf_2$, but the yields of these products are significantly lower (the same is indicated by $^1H$ NMR spectroscopy). The yield of $-CF_3$ substitution in the cation decreased 4-fold, and the yield of fragmentation also decreased. Radiolytic fragmentation of $Bz4MePy^+$ does not seem to be much affected by methyl substitution in BzPy $PF_6$ (Table 11S, Supporting Information). In both of these systems, there is a small yield of 4-methylpyridinium (ca. 0.015 and 0.12 molecules per 100 eV, respectively). It seems that the methyl substitution helps to protect the cation against substitution by anion fragments, but otherwise it does not significantly affect the fragmentation in a system (hexafluorophosphate) in which such damage is more important than substitution.

In contrast, 4-cyano substitution has a dramatic effect on cation stability in By4NCPy $NTf_2$, as a significant fraction of the cations releases cyanide. Apparently, the corresponding electron adduct can eliminate the $CN^-$ anion instead of forming a dimer complex or releasing the benzyl radical. Despite the existence of this new reaction channel, the yields of other radiolytic products (Tables 12S and 13S, Supporting Information) are not dramatically changed from the BzPy $NTf_2$ system.

To summarize this section, our product analyses corroborate the conclusions reached by spectroscopic means. 1-Benzylpyridinium cations and their 4-substituted derivatives demonstrate remarkable resistance to elimination of benzyl arms and carbon-1′ substitution in these arms. The extent of cation fragmentation is not greatly affected by variations of the counteranion; in contrast, substitution (by anion fragments) is greatly affected by such variations. It follows that anion fragmentation and the subsequent cation modification determine the overall radiation stability in these systems, while *the fragmentation of the cation is not a primary concern.*

**3.4. Computational Analysis.** We reach the conclusion that *cation stability to fragmentation is determined by the primary reactions at an early stage of radiolysis rather than secondary reactions (that lead to cation substitution)*. For this reason, we can focus exclusively on this primary chemistry, which is fortuitous as our spectroscopic observations aid us only in providing information about this primary chemistry. Section 3.1 and ref 1 informed us about the principal difference between $BzPy^+$ and $BzMeIm^+$ systems. In the latter, reduction of the cation results in a loss of the benzyl arm; in the former, this reaction does not occur. Product analyses indicate that the loss of the benzyl arm (both as a carbocation and a radical) is negligible.

No spectroscopic signatures of pyridinyl radicals were observed in irradiated pyridinium compounds (section 3.1). According to our DFT calculations, in gas-phase $BzPy^\bullet$, the elimination of $Bz^\bullet$ would be exergonic by 69 meV, so it is a marginally bound species (yet experimentally the benzyl radicals were not observed). In contrast, in gas-phase $EtPy^\bullet$, the elimination of the ethyl radical is estimated to be endergonic by 0.54 eV; thus, the corresponding pyridinyl radical should be stable. However, no pyridinyl radical was observed in that system either. It was the presence of other pyridinium cations that made a crucial difference, and therefore, stability against fragmentation in the reduced species is achieved through the collective modes of electron localization reducing the weakening of the individual C(1′)−N bonds. The TA spectra (section 3.2) suggest that the electron can be shared by two units in a $\pi$-electron sandwich dimer radical ion. We cannot *prove* that this is the case; instead, we will demonstrate that this rationale is feasible and consistent with our observations.

$(HPy)_2^{+\bullet}$ is the simplest $\pi$-electron dimer of this type, and it is structurally similar to the much studied benzene dimer radical cation.[5−7,9,10,13−15] In the latter species, the $D_{6h}$ symmetry of the monomer is reduced to $D_{2h}$ by sliding of the two rings relative to each other and some longitudinal distortion (structure **a** in Figure 20S, Supporting Information);[14,15] the binding energy (BE) was estimated to be 0.85 eV[7,14] (our DFT estimates for centrosymmetric benzene and toluene dimer


dx.doi.org/10.1021/jp408242b | J. Phys. Chem. B 2013, 117, 14385−14399

radical cations are 0.76 and 0.69 eV, respectively), while experimental estimates cluster around 0.7−0.9 eV.

Figure 21S (Supporting Information) exhibits the optimized geometries for the $(HPy)_2^{+\bullet}$ dimer. As seen from this figure and Table 16S (Supporting Information), the $C_2$ symmetrical dimer (structure **b**) with tilted rings is the lowest energy conformer with a BE of 0.78 eV; however, the $C_{2h}$ symmetric dimer (structure **c**) with parallel rings separated by 2.93 Å (vs 3.45 Å in $(C_6H_6)_2^{+\bullet}$) is only 4 meV more energetic, and there are three other conformers within 50 meV. Thus, to the accuracy of DFT modeling, the bonding energy in $(HPy)_2^{+\bullet}$ is comparable to that in the aromatic dimer radical cations. Table 16S (Supporting Information) indicates halving of isotropic hfcc's for $^{14}N$ nuclei and the protons other than $^1H(N)$ in $(HPy)_2^{+\bullet}$ as compared to $HPy^{\bullet}$ (Table 4S, Supporting Information). Such halving is typical for other $\pi$-electron sandwich dimer radical cations of aromatic molecules.[9,10] These hfcc's only weakly depend on the symmetry of the dimer radical cation (Table 16S, Supporting Information). Simulations of EPR spectra of $(HPy)_2^{+\bullet}$ using these estimated hfcc's yield a Gaussian line with a peak-to-peak interval ($\Delta B_{pp}$) of 17.8 G. When the DFT calculations were carried out for $(MePy)^{+\bullet}$ dimer cations (Figure 21S, Supporting Information), the two lowest energy conformers were also $C_2$ and $C_{2h}$ symmetric that were also very close in energy (with BEs of 0.721 and 0.715 eV, respectively). Both of these structures yield halved hfcc's and a Gaussian resonance line (Table 16S, Supporting Information). The repulsion between the methyl groups is minimized by outward pointing, as in $(toluene)_2^{+\bullet}$,[10] and the BE is not greatly reduced by methyl substitution.

Since inspection of all possible conformers of $(BzPy)_2^{+\bullet}$ was computationally prohibitive, our examination was restricted to the $C_{2h}$ symmetrical structures (that for the other two dimer radical cations were within 5−6 meV from the lowest energy $C_2$ symmetrical structures). According to our DFT calculations (structure **a** in Figures 6 and 22S, Supporting Information), the lowest energy conformer has a binding energy of 0.57 eV in the gas phase. This folded structure is only 5 meV less energetic than structure **b** shown in Figure 22S (Supporting Information), in which the benzyl arms are outbound. Given the small differences in energy, the dimer radical cation in the IL is likely to be sampling several conformations, which qualitatively accounts for its weak CR band. Though the BE for $(BzPy)_2^{+\bullet}$ is lower in comparison to $(MePy)_2^{+\bullet}$, it remains >0.5 eV regardless of the conformation. The hfcc's for nitrogen-14 and protons in this dimer cation are similar for all of these conformers (Table 16S, Supporting Information), and simulated EPR spectra are Gaussian lines with $\Delta B_{pp}$ of 17.3 G (Figure 7). The hfcc's in the $^1H(1')$ protons are small (1.8−1.9 G) and the ones in the phenyl ring are negligible, so $d_7$ substitution has little effect on this resonance line, whereas $d_5$ substitution narrows it down considerably, as demonstrated by the simulations in Figure 7. To contrast the difference with the monomer, in Figure 7, we also plotted EPR spectra for two conformers of the tentative pyridinyl radical in all four isotopic configurations.

The conformations of 1-benzylpyridinium (that has mirror symmetry) can be classified by the angle that two aromatic rings make with the N(1)−C(1′)−C(2′) plane: these rings can be either perpendicular to this plane (o) or lie on the plane (i); in the following, the orientation of the pyridinium ring is given first. Since the (i,i) conformer is sterically hindered, there is an elbow (o,o) and two propeller conformers, (i,o) and (o,i). Our

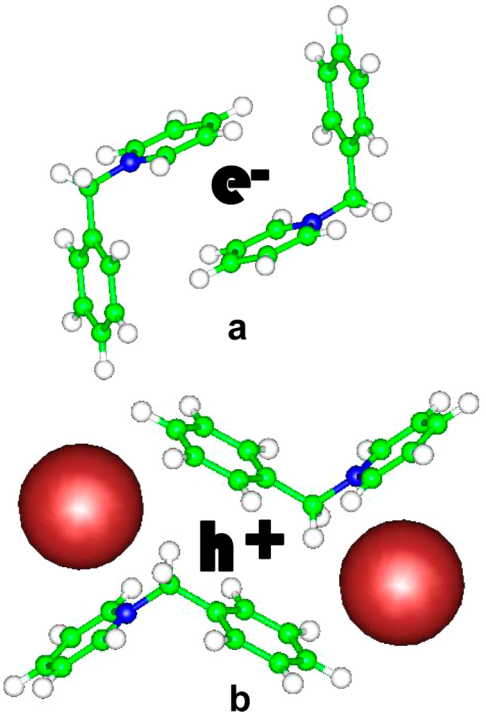


**Figure 6.** Geometry optimized $C_{2h}$ symmetrical structures for (o,o) conformers of (a) $(BzPy)_2^{+\bullet}$ and (b) $(BzPy)_2^{3+\bullet}$ (in the latter, the positions of chloride counteranions are also indicated). These two structures represent $\pi$−electron dimer radical ions (trapped electron and hole centers, respectively, in the irradiated 1-benzylpyridinium compounds).

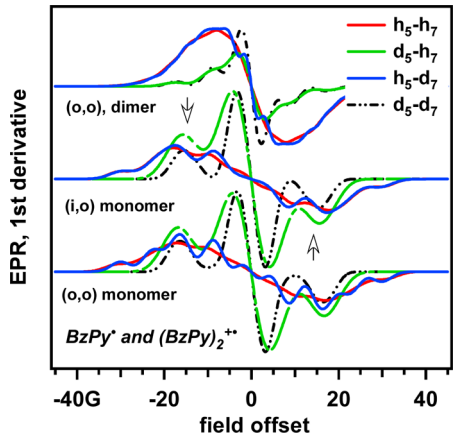


**Figure 7.** Simulated first-derivative EPR spectra for $(BzPy)_2^{+\bullet}$ (for a species shown in Figure 6) compared to the two lowest energy conformers of the pyridinyl radical. The isotopomers are indicated in the plot, and the arrows indicate the outer lines split by interaction of the unpaired electron with the $^{14}N$ nucleus. As the largest hfcc's are in the pyridinium group (Tables 4S and 16S, Supporting Information), these EPR spectra are weakly sensitive to $d_7$ substitution in the benzyl group.

DFT calculations (Table 4S, Supporting Information) indicate that the (i,o) conformation is the most stable for the parent cation; however, the (o,o) configuration is only 31 meV higher in energy and the (o,i) configuration is 100 meV higher in energy, so the rotation of the aromatic rings in $BzPy^+$ is relatively free. In $BzPy^{\bullet}$, the (o,o) and (o,i) conformers are close in energy (within 20 meV) and bound (it is their EPR spectra that are shown in Figure 7), whereas the (o,i)


dx.doi.org/10.1021/jp408242b | J. Phys. Chem. B 2013, 117, 14385−14399

conformer dissociates at the N(1)−C(1′) bond, releasing the benzyl radical. The latter release is exergonic for the $BzPy^{\bullet}$ and $Bz4MePy^{\bullet}$ radicals (by 70 and 140 meV, respectively) but endergonic for the $Bz4NCPy^{\bullet}$ radical (by 380 meV). The C(1′)−N bond dissociation energies (BDEs) for the corresponding cations are 2.18, 2.35, and 1.75 eV, respectively, so the increase in the stability of the pyridinyl radical anticorrelates with the stability of the excited cation to carbocation elimination. For other radicals of interest (such as H atom adducts, Table 6S, Supporting Information), the (i,o) conformations are the lowest in energy, with the exception of $BzPy^{2+\bullet}$ and −H(1′) loss radicals, for which the (o,i) conformation is preferred due to the alignment of the C 2p orbital with $\pi$-orbitals in the benzyl ring (Tables 4S and 6S, Supporting Information). As this (o,i) radical is the highest energy conformer of the parent cation, there is an additional reaction barrier to H(1′) atom elimination or deprotonation (that requires ring rotation).

As seen in Figure 6, in the $(BzPy)_2^{+\bullet}$ dimers, the BzPy units are locked in (o,o) conformations, as the dissociative (o,i) conformations are energetically prohibited in the dimer due to the increased repulsion between the benzyl and pyridinium groups. Since the C(1′)−N bond dissociation is nearly thermoneutral even in the pyridinyl radical (as it involves a small activation barrier in the lowest energy conformer), this conformation locking and interaction between the two units may be sufficient to prevent benzyl radical loss in the dimer radical cation as opposed to the monomer radical. For $BzMeIm^{+}$, the formation of the $\pi$-electron sandwich dimer cation does not occur,[1] and the elimination of the benzyl radical proceeds unimpeded.

Equally remarkable is that low-temperature EPR spectra do not indicate significant H(1′) and H(5′) loss, while such H loss is typical for aromatic cations with *alkyl* side arms. Instead, it appears that the EPR spectra are dominated by an almost featureless line that transforms to a narrower line after $d_7$-substitution. The H loss radical is the product of deprotonation of the trapped hole, which is the radical dication $BzPy^{2+\bullet}$. As we argued in section 3.2, a strong CR band in the NIR from a hole center (very similar to that for irradiated benzene and toluene) that is observed in BzPy $NTf_2$ indicates that hole centers in this IL stabilize as $(BzPy)_2^{3+\bullet}$ trications, in which the charge and spin are divided between the phenyl groups in a dimer.

In $D_{2h}$ symmetrical $(C_6H_6)_2^{+\bullet}$ that has a CR band centered at 920 nm,[5,8,60] the calculated proton hfcc's for four $^1H(1,4)$ protons (along the long axis) are −5.9 G and the other protons have hfcc's of −0.76 G.[9] Due to rapid pseudorotation in the $(C_6H_6)_2^{+\bullet}$ dimer, all protons are in fact magnetically equivalent with a mean hfcc of 2.15 G. In a centrosymmetrical $(toluene)_2^{+\bullet}$ dimer that has the CR band centered at 1020 nm,[5,60] there are two strongly coupled $^1H(4)$ protons (~4.64 G) and six methyl protons with a hfcc of 7.46 G.[10] From these results, one may expect relatively large hfcc's in $^1H(1′)$ and $^1H(5′)$ protons in $(BzPy)_2^{3+\bullet}$ corresponding to approximately half of the hfcc's for the respective protons in $BzPy^{2+\bullet}$ (Tables 16S and 4S, Supporting Information). In the latter, the hfcc's for two $^1H(1′)$ protons very strongly depend on the conformation as the benzyl group rotates around the C(1′)−C(2′) axis, changing from 21.3 G in (o,i) (the lowest energy conformer) to 3.9 G in (o,o) (which is 160 meV more energetic). Given the small rotation barriers, the conformation of the benzyl arm in the dimer trication may not be well fixed, which creates difficulty in estimating hfcc's in the bridging methylene groups.

To obtain an estimate, we optimized the geometry of two $C_{2h}$ symmetrical (o,o) conformers of the $(BzPy\cdots Cl)_2^{+\bullet}$ cation (Figures 6 and 23S, Supporting Information) and then replaced the chloride anions with point negative charges and calculated the corresponding hfcc's. The structure with the counteranions on the periphery (structure **b** in Figure 6) and the two phenyl rings separated by 3.93 Å has the lowest energy. As seen from Table 16S (Supporting Information), hfcc's for $^{14}N$ and $^1H$ nuclei in this structure are very close to the halved hfcc's for the (o,o) conformer of $BzPy^{2+\bullet}$. Since the hfcc's for protons in the pyridinium group are negligible, this calculation suggests that $h_7-h_5$ and $h_7-d_5$ isotopomers of $(BzPy)_2^{3+\bullet}$ have identical EPR spectra; the corresponding $d_7$ isotopomers, in contrast, have EPR spectra corresponding to a narrow Gaussian line. On the other hand, simulations in Figure 7 indicate that EPR spectra of $h_7-h_5$ and $d_7-h_5$ isotopomers of $(BzPy)_2^{+\bullet}$ are very similar; i.e., the two centers follow different trends on isotope substitution.

Assuming that the prevalent spin centers in irradiated BzPy $NTf_2$ are these dimer cations, the total EPR spectrum of the $d_7-h_5$ isotopomer is a superposition of a narrow line from the $d_7$ isotopomer of $(BzPy)_2^{3+\bullet}$ and a broader line from the $h_7$ isotopomer of $(BzPy)_2^{+\bullet}$. In Figure 24S (Supporting Information), we compare magnified wings of the EPR spectrum for the $d_7-h_5$ isotopomer to the EPR spectrum for the $h_7-h_5$ isotopomer. It is observed that the two are identical, so this feature should be dominated by the $(BzPy\text{-}h_5)_2^{+\bullet}$ resonances. Conversely, the comparison of EPR spectra for $h_7-h_5$ and $h_7-d_5$ isotopomers indicates envelope narrowing after $d_5$-substitution. The latter EPR spectrum should be dominated by $(Bz\text{-}h_7-Py)_2^{3+\bullet}$ resonances in the wings and by the collapsed, narrow line of $(Bz\text{-}d_7-Py)_2^{+\bullet}$ at the center. These comparisons suggest that the hole center has an ~20% narrower envelope than the electron center. The latter is also suggested by the similarity of the EPR spectra for the $h_7-h_5$ isotopomers of BzPy $NTf_2$ and BzPy Cl (Figure 8). In the latter, the holes are trapped as $Cl_2^{-\bullet}$ rather than $(BzPy)_2^{3+\bullet}$ centers, and the resonance line should arise mainly from the trapped electron center, $(BzPy)_2^{+\bullet}$.

In Figure 8, we overlap simulated and experimental EPR spectra using hfcc parameters computed for the dimer species shown in Figure 6. Our calculations do yield a narrower envelope for the hole center as compared to the electron center; the overall agreement is good. However, to achieve this agreement, we needed to scale down the offset field by a factor of 1.25; i.e., our gas-phase calculations underestimate the widths of the EPR spectra. The likely cause of this discrepancy is conformational variation in hfcc's for $^1H(1)$ protons that is apparent in our DFT calculations. Given the small differences in the conformational energies, this is an effect which is particularly challenging to reproduce by computational modeling, as both this conformational dynamics and the energetics are strongly affected by the environment. Excluding this complication, $\pi$-electron dimer ions consistently account for our experimental results.

## 4. CONCLUDING REMARKS

In order to viably replace conventional molecular diluents in nuclear separations, hydrophobic ionic liquids (ILs)[58] should be stabilized to radiolytic decomposition.[26,30,31,53,54,61−63] This study supports previous results[18,54−56,58,59,64,65] in singling out anion instability as the main culprit: the cations in ILs become

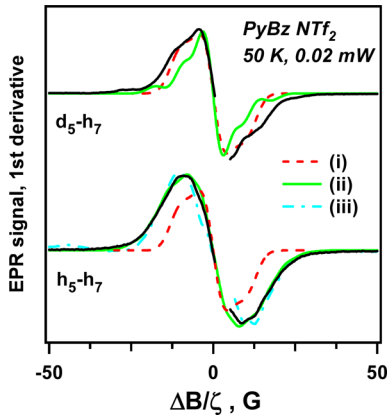


**Figure 8.** The comparison of simulated first-derivative EPR spectra for structures shown in Figure 6 and the experimental EPR spectrum of irradiated BzPy $NTf_2$ from Figure 1. The electron (i) and hole (ii) centers are shown for $h_7-h_5$ and $h_7-d_5$ isotopomers of 1-benzylpyridinium. Trace (iii) is the EPR spectrum obtained for irradiated Bz-$h_7$–Py-$h_5$ Cl, in which the hole is trapped as the $Cl_2^{-\bullet}$ center (the resonance lines of the latter do not overlap with the line of the trapped-electron center; see Figure 6S, Supporting Information). In the experimental spectra, the field offset $\Delta B$ was scaled by a factor of $\zeta$ = 1.25 (see the text).

substituted by fragment radicals generated in decomposition of the constituent anions. In addition to such reactions, the cations also undergo fragmentation that results in the loss of their side arms. Our aim is to develop approaches to improving cation stability in such fragmentation reactions. Although such undesirable reactions cannot be entirely suppressed, it is possible to decrease their extent to a degree when such decomposition is negligible over the expected life cycle of the IL diluent. Our mechanistic insight is threefold:

First, we demonstrated that, by stabilization of the carbocation released in the dissociation of the electronically excited cations, it is possible to reverse this channel of cation fragmentation.

Second, using 1-benzylpyridinium ILs as an example, we have shown that charge delocalization significantly reduces the efficiency of fragmentation in oxidized and reduced states of the cation. Reduced pyridinium cations form a $\pi$-electron sandwich dimer with the parent cation in which the positive charge and spin are shared between two *pyridinium* moieties. This mode of electron localization appears to be specific to pyridinium cations and it qualitatively accounts for the stability of such cations to elimination of benzyl arms in their reduced form, while this elimination is energetically favorable in a monomer (pyridinyl) radical. For aromatic cations in which this stabilization does not occur (such as 1-benzyl-3-methylimidazolium), this elimination is facile even at low temperature.

For cations containing benzyl groups, we have observed another stabilization mechanism that involves oxidized cations (holes), namely, the formation of dimers involving their *phenyl* moieties. This stabilization results in lower yields of deprotonation, which also contributes to improved radiation stability of the $BzPy^+$ cation. In fact, product analyses indicate that deprotonation from the $\alpha$-carbon site is entirely suppressed. In this regard, 1-benzylpyridinium and its substituted derivatives appear to be unique, as there is stabilization of *both* the oxidized and reduced cations through charge sharing.

It has already been hypothesized that ILs consisting of 6-member-ring aromatic cations may support uncommon modes of excess charge localization,[41,42] but no experimental evidence was produced. Our results show not only that such charge delocalization is possible but that it is the key to increasing the radiation stability of ILs. Improved insight into the details of excess charge distribution in ILs would bring considerable benefits in addressing a problem of great practical importance, and we urge further theoretical and experimental studies in this area. Although our picture of charge delocalization broadly agrees with the results of transient absorption spectroscopy, EPR, and product analyses, the exact fashion of this delocalization remains tentative, as is also the case for many molecular solvents.[66,67]

Third, while such charge delocalization is beneficial, it is not the only approach to improving cation stability. As was noted, the stability of the electronically excited cations generally anticorrelates with the stability of their reduced states, and the electron delocalization addresses the latter. However, *the same end result can be obtained through competitive electron scavenging that precludes cation reduction.* In part 1,[1] we demonstrated this strategy for 1-benzyl-3-methylimidazolium, which promptly releases the benzyl radical when reduced. When this cation was paired with saccharinate (that preferentially accepts electrons in this system), the fragmentation of the cation was prevented. More importantly, introduction of a protic impurity was also sufficient to inhibit the fragmentation.

In a practical setting, the IL diluent always remains in contact with the aqueous raffinate. The acidity of the latter alternates between two extremes during the forward and back extractions,[53,68] so the IL diluent may spend roughly half of its life cycle in contact with acidic (typically, nitric acid) aqueous solutions. As nitric acid and nitrate are very efficient electron scavengers, most radiolytically generated electrons are scavenged by hydronium ions and nitric acid/nitrate introduced into the IL.[57] In this part of the cycle, the reductive channel to cation fragmentation does not pose a problem. It should be noted that such acid dopants can protonate bases released in reaction 1b, suppressing reverse reaction 3b. As the latter is a geminate reaction, such interference can occur only when the concentration of the acid is very high, which is only possible when the IL diluent is in contact with concentrated acid solutions. Since the nitrate and nitric acid also serve as efficient quenchers of electronic excitation,[57] they will also suppress reaction 3a, so radiolytic fragmentation of cations in highly acidic ILs is also unlikely to be a problem. However, as the proticity alternates between extremes during the forward and back extractions, the IL diluent also needs to be stabilized to radiation damage under the conditions of low acidity. The reliance on energy quenchers and electron scavengers introduced into the IL diluent form the aqueous raffinate cannot extend to the other extreme. For this latter regime, the intrinsic resistance of the IL to radiation becomes important, and this study suggests several ways in which it can be improved.

Our study has another interesting facet. Recently, it has been proposed that pyridinyl radicals may be key intermediates in electrochemical fixation of $CO_2$,[69,70] although this role has been disputed.[71,72] The revealed tendency of the tentative pyridinyl radicals to form a sandwich complex with its parent cation may have a significant effect on the energetics and reactivity of such radicals.


dx.doi.org/10.1021/jp408242b | J. Phys. Chem. B 2013, 117, 14385−14399

## ■ ASSOCIATED CONTENT

### Supporting Information

A PDF file containing a list of abbreviations, synthetic procedures (section 1S), Tables 1S−16S, and Figures 1S−24S with captions, including the experimental and simulated EPR spectra, NMR and MS data, and DFT calculations. This material is available free of charge via the Internet at http://pubs.acs.org.

## ■ AUTHOR INFORMATION


### Corresponding Author

*E-mail shkrob@anl.gov. Phone: (630) 252-9516.

### Present Addresses

[⊥]Department of Chemistry and Biochemistry, Hunter College, CUNY, 695 Park Ave, New York, NY 10021.

[#]Department of Radiation Chemistry and Technology, Institute of Nuclear Chemistry and Technology, Dorodna 16, 03-195 Warsaw, Poland.


### Notes

The authors declare no competing financial interest.

## ■ ACKNOWLEDGMENTS


We thank S. Chemerisov, R. Lowers, D. Quigley, A. Kokhan, S. Lopykinski, and J. Muntean for technical support, R. D. Rimmer, P. Sreearunothai, and S. Oliveri for assistance, and P. Zapol and S. I. Lall-Ramnarine for many useful discussions. This work, and use of the LEAF Facility of the BNL Accelerator Center for Energy Research, was supported by the US-DOE Office of Science, Division of Chemical Sciences, Geosciences and Biosciences under Contract Nos. DE-AC02-06CH11357 (Argonne) and DE-AC02-98CH10886 (Brookhaven). Programmatic support via a DOE SISGR grant "An Integrated Basic Research Program for Advanced Nuclear Energy Separations Systems Based on Ionic Liquids" is gratefully acknowledged. T.S. was supported by LDRD Project 03-118 from Brookhaven National Laboratory.

We dedicate this study to the blessed memory of late Piotr Pieniazek who as a postdoctoral student of Profs. Stephen Bradforth and Anna Krylov at the University of Southern California made seminal contributions to theoretical understanding of sandwich dimer cations for aromatic molecules.


## ■ REFERENCES


(1) Shkrob, I. A.; Marin, T. W.; Luo, H.; Dai, S. Radiation Stability of Cations in Ionic Liquids. 1. Alkyl and Benzyl Derivatives of 5-Membered Ring Heterocycles. *J. Phys. Chem. B* **2013**, DOI: 10.1021/jp4082432.

(2) Barylyuk, K. V.; Chingin, K.; Balabin, R. M.; Zenobi, R. Fragmentation of Benzylpyridinium "Thermometer" Ions and Its Effect on the Accuracy of Internal Energy Calibration. *J. Am. Soc. Mass Spectrom.* **2010**, *21*, 172−177.

(3) Bobrowski, K. Pulse Radiolysis of Aqueous Solutions of Benzyltrialkylammonium Cations: Reactions with the Primary Transients from Water Radiolysis. *J. Phys. Chem.* **1981**, *85*, 381−388.

(4) Mittal, L. J.; Mittal, J. P. Site of Attack in the Interaction of Hydrated Electrons and Hydroxy Radicals in the Pulse Radiolysis of Arylalkylamines in Aqueous Solutions. *Radiat. Phys. Chem.* **1986**, *28*, 363−371.

(5) Badger, B.; Brocklehurst, B. Absorption Spectra of Dimer Cations. Part 2.—Benzene Derivatives. *Trans. Faraday Soc.* **1969**, *65*, 2582−2587.

(6) Badger, B.; Brocklehurst, B. Absorption Spectra of Dimer Cations. Part 4.—Theoretical Considerations and Dimer Structure. *Trans. Faraday Soc.* **1970**, *66*, 2939−2947.

(7) Grover, J. R.; Walters, E. A.; Hui, E. T. Dissociation Energies of the Benzene Dimer and Dimer Cation. *J. Phys. Chem.* **1987**, *91*, 3233−3237.

(8) Inokuchi, Y.; Naitoh, Y.; Ohashi, K.; Saitow, K.; Yoshihara, K.; Nishi, N. Formation of Benzene Dimer Cations in Neat Liquid Benzene Studied by Femtosecond Transient Absorption Spectroscopy. *Chem. Phys. Lett.* **1997**, *269*, 298−304.

(9) Kadam, R. K.; Erickson, R.; Komaguchi, K.; Shiotani, M.; Lund, A. ENDOR and EPR Studies of Benzene Radical Cations in Halocarbon Matrices: the Static Jahn−Teller Distortion of the Monomer and Geometry of the Dimer Cation. *Chem. Phys. Lett.* **1998**, *290*, 371−378.

(10) Itagaki, Y.; Benetis, N. P.; Kadam, R. K.; Lund, A. Structure of Dimeric Radical Cations of Benzene and Toluene in Halocarbon Matrices: an EPR, ENDOR and MO Study. *Phys. Chem. Chem. Phys.* **2000**, *2*, 2683−2689.

(11) Rusyniak, M.; Ibrahim, Y.; Alsharaeh, E.; Mautner, M.; Samy El-Shall, M. Mass-Selected Ion Mobility Studies of the Isomerization of the Benzene Radical Cation and Binding Energy of the Benzene Dimer Cation. Separation of Isomeric Ions by Dimer Formation. *J. Phys. Chem. A* **2003**, *107*, 7656−7666.

(12) Todo, M.; Okamoto, K.; Seki, S.; Tagawa, S. Formation of Benzene Trimer Radical Cation in Gamma-Irradiated Low Temperature 2-Methylpentane Matrices. *Chem. Phys. Lett.* **2004**, *399*, 378−383.

(13) Okamoto, K.; Seki, S.; Tagawa, S. Formation of Trimer and Dimer Radical Cations of Methyl-Substituted Benzenes in γ-Irradiated Low-Temperature Matrices. *J. Phys. Chem. A* **2006**, *110*, 8073−8080.

(14) Pieniazek, P. A.; Krylov, A. I.; Bradforth, S. E. Electronic Structure of the Benzene Dimer Cation. *J. Chem. Phys.* **2007**, *127*, 044317.

(15) Pieniazek, P. A.; Bradforth, S. E.; Krylov, A. I. Charge Localization and Jahn−Teller Distortions in the Benzene Dimer Cation. *J. Chem. Phys.* **2008**, *129*, 074104.

(16) Fujitsuka, M.; Tojo, S.; Shinmyozu, T.; Majima, T. Intramolecular Dimer Radical Anions of [3n] Cyclophanes: Transannular Distance Dependent Stabilization Energy. *Chem. Commun.* **2009**, 1553−1555.

(17) Lall-Ramnarine, S. I.; Castano, A.; Subramaniam, G.; Thomas, M. F.; Wishart, J. F. Synthesis, Characterization and Radiolytic Properties of Bis(oxalato)borate Containing Ionic Liquids. *Radiat. Phys. Chem.* **2009**, *78*, 1120−1125.

(18) Shkrob, I. A.; Marin, T. W.; Chemerisov, S. D.; Hatcher, J. L.; Wishart, J. F. Toward Radiation-Resistant Ionic Liquids. Radiation Stability of Sulfonyl Imide Anions. *J. Phys. Chem. B* **2012**, *116*, 9043−9055.

(19) Lee, C.; Yang, W.; Parr, R. G. Development of the Colle-Salvetti Correlation-Energy Formula into a Functional of the Electron Density. *Phys. Rev. B* **1988**, *37*, 785−789.

(20) Becke, A. D. Density-Functional Exchange-Energy Approximation with Correct Asymptotic Behavior. *Phys. Rev. A* **1988**, *38*, 3098−3100.

(21) Frisch, M. J.; Trucks, G. W.; Schlegel, H. B.; Scuseria, G. E.; Robb, M. A.; Cheeseman, V. G.; Montgomery, J. A., Jr.; Vreven, K. N.; Kudin, J. C.; Burant, J. C. *Gaussian 03*, rev. C.02; Gaussian, Inc.: Wallingford, CT, 2004.

(22) Wishart, J. F.; Cook, A. R.; Miller, J. R. The LEAF Picosecond Pulse Radiolysis Facility at Brookhaven National Laboratory. *Rev. Sci. Instrum.* **2004**, *75*, 4359−4366.

(23) Wishart, J. F.; Funston, A. M.; Szreder, T.; Cook, A. R.; Gohdo, M. Electron Solvation Dynamics and Reactivity in Ionic Liquids Observed by Picosecond Radiolysis Techniques. *Faraday Discuss.* **2012**, *154*, 353−363.

(24) Cook, A. R.; Shen, Y. Z. Optical Fiber-Based Single-Shot Picosecond Transient Absorption Spectroscopy. *Rev. Sci. Instrum.* **2009**, *80*, 073106.

(25) Mahurin, S. M.; Dai, T.; Yeary, J. S.; Luo, H. M.; Dai, S. Benzyl-Functionalized Room Temperature Ionic Liquids for $CO_2/N_2$ Separation. *Ind. Eng. Chem. Res.* **2011**, *50*, 14061−14069.

(26) Shkrob, I. A.; Wishart, J. F. Free Radical Chemistry in Room-Temperature Ionic Liquids. In *Encyclopedia of Radicals in Chemistry, Biology and Materials*; Chatgilialoglu, C., Studer, A., Eds.; John Wiley & Sons, Ltd.: Chichester, U.K., 2012; pp 433−448.
(27) Skrzypczak, A.; Neta, P. Diffusion-Controlled Electron-Transfer Reactions in Ionic Liquids. *J. Phys. Chem. A* **2003**, *107*, 7800−7803.
(28) Shkrob, I. A.; Chemerisov, S. D.; Wishart, J. F. The Initial Stages of Radiation Damage in Ionic Liquids and Ionic Liquid-Based Extraction Systems. *J. Phys. Chem. B* **2007**, *111*, 11786−11793.
(29) Shkrob, I. A.; Marin, T. W.; Chemerisov, S. D.; Hatcher, J. L.; Wishart, J. F. Radiation Induced Redox Reactions and Fragmentation of Constituent Ions in Ionic Liquids. 2. Imidazolium Cations. *J. Phys. Chem. B* **2011**, *115*, 3889−3902.
(30) Wishart, J. F.; Shkrob, I. A. The Radiation Chemistry of Ionic Liquids and Its Implications for Their Use in Nuclear Fuel Processing. In *Ionic Liquids: From Knowledge to Application*; Plechkova, N. V., Rogers, R. D., Seddon, K. R., Eds.; American Chemical Society: Washington, DC, 2009; pp 119−134.
(31) Wishart, J. F. Ionic Liquids and Ionizing Radiation: Reactivity of Highly Energetic Species. *J. Phys. Chem. Lett.* **2010**, *1*, 3225−3231.
(32) Muller, E. A.; Strader, M. L.; Johns, J. E.; Yang, A.; Caplins, B. W.; Shearer, A. J.; Suich, D. E.; Harris, C. B. Femtosecond Electron Solvation at the Ionic Liquid/Metal Electrode Interface. *J. Am. Chem. Soc.* **2013**, *135*, 10646−10653.
(33) Shkrob, I. A.; Wishart, J. F. Charge Trapping in Imidazolium Ionic Liquids. *J. Phys. Chem. B* **2009**, *113*, 5582−5592.
(34) Wishart, J. F.; Neta, P. Spectrum and Reactivity of the Solvated Electron in the Ionic Liquid Methyltributylammonium Bis-(trifluoromethylsulfonyl)imide. *J. Phys. Chem. B* **2003**, *107*, 7261−7267.
(35) Wishart, J. F.; Lall-Ramnarine, S. I.; Raju, R.; Scumpia, A.; Bellevue, S.; Ragbir, R.; Engel, R. Effects of Functional Group Substitution on Electron Spectra and Solvation Dynamics in a Family of Ionic Liquids. *Radiat. Phys. Chem.* **2005**, *72*, 99−104.
(36) Asano, A.; Yang, J.; Kondoh, T.; Norizawa, K.; Nagaishi, R.; Takahashi, K.; Yoshida, Y. Molar Absorption Coefficient and Radiolytic Yield of Solvated Electrons in Diethylmethyl(2-methoxy)-ammonium Bis(trifluoromethanesulfonyl)imide Ionic Liquid. *Radiat. Phys. Chem.* **2008**, *77*, 1244−1247.
(37) Takahashi, K.; Sato, T.; Katsumura, Y.; Yang, J.; Kondoh, T.; Yoshida, Y.; Katoh, R. Reactions of Solvated Electrons with Imidazolium Cations in Ionic Liquids. *Radiat. Phys. Chem.* **2008**, *77*, 1239−1243.
(38) Behar, D.; Gonzalez, C.; Neta, P. Reaction Kinetics in Ionic Liquids: Pulse Radiolysis Studies of 1-Butyl-3-methylimidazolium Salts. *J. Phys. Chem. A* **2001**, *105*, 7607−7614.
(39) Marcinek, A.; Zielonka, J.; Gebicki, J.; Gordon, C. M.; Dunkin, I. R. Ionic Liquids: Novel Media for Characterization of Radical Ions. *J. Phys. Chem. A* **2001**, *105*, 9305−9309.
(40) Behar, D.; Neta, P.; Schultheisz, C. Reaction Kinetics in Ionic Liquids as Studied by Pulse Radiolysis: Redox Reactions in the Solvents Methyltributylammonium Bis(trifluoromethylsulfonyl)imide and *N*-Butylpyridinium Tetrafluoroborate. *J. Phys. Chem. A* **2002**, *106*, 3139−3147.
(41) Wang, Z. P.; Zhang, L.; Chen, X. H.; Cukier, R. I.; Bu, Y. X. Excess Electron Solvation in an Imidazolium-Based Room-Temperature Ionic Liquid Revealed by Ab Initio Molecular Dynamics Simulations. *J. Phys. Chem. B* **2009**, *113*, 8222−8226.
(42) Wang, Z.; Zhang, L.; Cukier, R. I.; Bu, Y. States and Migration of an Excess Electron in a Pyridinium-Based, Room-Temperature Ionic Liquid: an *ab Initio* Molecular Dynamics Simulation Exploration. *Phys. Chem. Chem. Phys.* **2010**, *12*, 1854−1861.
(43) Funston, A. M.; Fadeeva, T. A.; Wishart, J. F.; Castner, E. W. Fluorescence Probing of Temperature-Dependent Dynamics and Friction in Ionic Liquid Local Environments. *J. Phys. Chem. B* **2007**, *111*, 4963−4977.
(44) Margulis, C. J.; Annapureddy, H. V.; De Biase, P. M.; Coker, D.; Kohanoff, J.; Del Pópolo, M. G. Dry Excess Electrons in Room-Temperature Ionic Liquids. *J. Am. Chem. Soc.* **2011**, *133*, 20186−20193.
(45) Since we do not yet know the extinction coefficients of the trapped-charge state absorption spectra in the benzyl-substituted ILs, we cannot reliably estimate radiolytic yields. A reasonable extinction coefficient for CR states like these would be $6 \times 10^3$ $M^{-1}$ $cm^{-1}$, while that of the solvated electron in $C_4$mpyrr $NTf_2$ is $\sim 2.2 \times 10^4$ $M^{-1}$ $cm^{-1}$ at 1.1 $\mu$m (which corresponds to ∼1.0 per 100 eV). It appears that observed G$\varepsilon$ values of the CR state yields are higher than the solvated electron yield in $C_4$mpyrr $NTf_2$.
(46) Tojo, S.; Fujitsuka, M.; Majima, T. Intramolecular Charge Resonance in Dimer Radical Anions of Di-, Tri-, Tetra-, and Pentaphenylalkanes. *J. Org. Chem.* **2012**, *77*, 4932−4938.
(47) Anthony, J. L.; Anderson, J. L.; Maginn, E. J.; Brennecke, J. F. Anion Effects on Gas Solubility in Ionic Liquids. *J. Phys. Chem. B* **2005**, *109*, 6366−6374.
(48) Shiflett, M. B.; Niehaus, A. M. S.; Elliott, B. A.; Yokozeki, A. Phase Behavior of $N_2O$ and $CO_2$ in Room-Temperature Ionic Liquids Bmim $Tf_2N$, Bmim $BF_4$, Bmim $N(CN)_2$, Bmim Ac, Eam $NO_3$, and Bmim SCN. *Int. J. Thermophys.* **2012**, *33*, 412−436.
(49) Almantariotis, D.; Stevanovic, S.; Fandino, O.; Pensado, A. S.; Padua, A. A. H.; Coxam, J. Y.; Gomes, M. F. C. Absorption of Carbon Dioxide, Nitrous Oxide, Ethane and Nitrogen by 1-Alkyl-3-methylimidazolium ($C_n$mim, n = 2,4,6) Tris(pentafluoroethyl)-trifluorophosphate Ionic Liquids (eFAP). *J. Phys. Chem. B* **2012**, *116*, 7728−7738.
(50) Stevanovic, S.; Gomes, M. F. C. Solubility of Carbon Dioxide, Nitrous Oxide, Ethane, and Nitrogen in 1-Butyl-1-methylpyrrolidinium and Trihexyl(tetradecyl)phosphonium Tris(pentafluoroethyl)-trifluorophosphate (eFAP) Ionic Liquids. *J. Chem. Thermodyn.* **2013**, *59*, 65−71.
(51) Choudhury, A. R.; Winterton, N.; Steiner, A.; Cooper, A. I.; Johnson, K. A. In Situ Crystallization of Low-Melting Ionic Liquids. *J. Am. Chem. Soc.* **2005**, *127*, 16792−16793.
(52) Kashyap, H. K.; Santos, C. S.; Murthy, N. S.; Hettige, J. J.; Kerr, K.; Ramati, S.; Gwon, J.; Gohdo, M.; Lall-Ramnarine, S. I.; Wishart, J. F.; Margulis, C. J.; Castner, E. W. Structure of 1-Alkyl-1-methylpyrrolidinium Bis(trifluoromethylsulfonyl)amide Ionic Liquids with Linear, Branched, and Cyclic Alkyl Groups. *J. Phys. Chem. B* **2013**, DOI: 10.1021/jp403518j.
(53) Berthon, L.; Chabronnel, M.-C. Radiolysis of Solvents Used in Nuclear Fuel Reprocessing. In *Ion Exchange and Solvent Extraction, A Series of Advances*; Moyer, B. A., Ed.; CRC Press: Boca Raton, FL, 2010; Vol. *19*, pp 429−513.
(54) Berthon, L.; Nikitenko, S. I.; Bisel, I.; Berthon, C.; Faucon, M.; Saucerotte, B.; Zorz, N.; Moisy, P. Influence of Gamma Irradiation on Hydrophobic Room-Temperature Ionic Liquids [BuMeIm]$PF_6$ and [BuMeIm]$(CF_3SO_2)_2N$. *Dalton Trans.* **2006**, 2526−2534.
(55) Bosse, E.; Berthon, L.; Zorz, N.; Monget, J.; Berthon, C.; Bisel, I.; Legand, S.; Moisy, P. Stability of [$MeBu_3N$][$Tf_2N$] under Gamma Irradiation. *Dalton Trans.* **2008**, 924−931.
(56) Le Rouzo, G.; Lamouroux, C.; Dauvois, V.; Dannoux, A.; Legand, S.; Durand, D.; Moisy, P.; G., M. Anion Effect on Radiochemical Stability of Room-Temperature Ionic Liquids under Gamma Irradiation. *Dalton Trans.* **2009**, 6175−6184.
(57) Shkrob, I. A.; Marin, T. W.; Chemerisov, S. D.; Wishart, J. F. Radiation and Radical Chemistry of $NO_3^-$, $HNO_3$, and Dialkylphosphoric Acids in Room-Temperature Ionic Liquids. *J. Phys. Chem. B* **2011**, *115*, 10927−10942.
(58) Shkrob, I. A.; Marin, T. W.; Chemerisov, S. D.; Wishart, J. F. Radiation Induced Redox Reactions and Fragmentation of Constituent Ions in Ionic Liquids. 1. Anions. *J. Phys. Chem. B* **2011**, *115*, 3872−3888.
(59) Shkrob, I. A.; Marin, T. W.; Wishart, J. F. Ionic Liquids Based on Polynitrile Anions: Hydrophobicity, Low Proton Affinity, and High Radiolytic Resistance Combined. *J. Phys. Chem. B* **2013**, *117*, 7084−7094.
(60) Shida, T. *Electronic Absorption Spectra of Radical Ions*; Elsevier: Amsterdam, The Netherlands, 1988.

(61) Allen, D.; Baston, G.; Bradley, A. E.; Gorman, T.; Haile, A.; Hamblett, I.; Hatter, J. E.; Healey, M. J. F.; Hodgson, B.; Lewin, R.; Lovell, K. V.; Newton, B.; Pitner, W. R.; Rooney, D. W.; Sanders, D.; Seddon, K. R.; Sims, H. E.; Thied, R. C. An Investigation of the Radiochemical Stability of Ionic Liquids. *Green Chem.* **2002**, *4*, 152−158.
(62) Wishart, J. F. Radiation-Induced Reactivity in Ionic Liquids. *Houshasen Kagaku* **2011**, *91*, 39−43.
(63) Wishart, J. F. Ionic Liquid Radiation Chemistry. In *Ionic Liquids: COILed for Action*; Seddon, K. R., Rogers, R. D., Eds.; Wiley, Ltd.: Chichester, U.K., 2013; in press.
(64) Huang, W.; Chen, S.; Liu, Y.; Fu, H.; Wu, G. Fluoride Ion Yield and Absorption Spectral Analysis of Irradiated Imidazolium-Based Room-Temperature Ionic Liquids. *Radiat. Phys. Chem.* **2011**, *80*, 573−577.
(65) Sun, T.; Shen, X.; Chen, Q.; Ma, J.; Zhang, S.; Huang, J. Identification of $F^-$ and $SO_4^{2-}$ as the Radiolytic Products of the Ionic Liquid $C_4$mim $NTf_2$ and Their Effect on the Extraction of $UO_2^{2+}$. *Radiat. Phys. Chem.* **2013**, *83*, 74−78.
(66) Shkrob, I. A.; Sauer, M. C. Radical Ions in Liquids. In *Charged Particle and Photon Interactions with Matter. Chemical, Physicochemical, and Biological Consequences with Applications*; Mozumder, Y. H. a. A., Ed.; Marcel Dekker: New York, 2004; pp 301−331.
(67) Shkrob, I. A. The Structure and Dynamics of Solvated Electrons. In *Recent Trends in Radiation Chemistry*; Wishart, J. F., Rao, B. S. M., Eds.; World Scientific Publishing: Singapore, 2010; pp 59−97.
(68) Marin, T. W.; Shkrob, I. A.; Dietz, M. L. Hydrogen-Bonding Interactions and Protic Equilibria in Room-Temperature Ionic Liquids Containing Crown Ethers. *J. Phys. Chem. B* **2011**, *115*, 3912−3918.
(69) Barton, E. E.; Rampulla, D. M.; Bocarsly, A. B. Communication Selective Solar-Driven Reduction of $CO_2$ to Methanol Using a Catalyzed p-GaP Based Photoelectrochemical Cell. *J. Am. Chem. Soc.* **2008**, *130*, 6342−6344.
(70) Barton Cole, E.; Lakkaraju, P. S.; Rampulla, D. M.; Morris, A. J.; Abelev, E.; Bocarsly, A. B. Using a One-Electron Shuttle for the Multielectron Reduction of $CO_2$ to Methanol: Kinetic, Mechanistic, and Structural Insights. *J. Am. Chem. Soc.* **2010**, *132*, 11539−11551.
(71) Keith, J. A.; Carter, E. A. Theoretical Insights into Pyridinium-Based Photoelectrocatalytic Reduction of $CO_2$. *J. Am. Chem. Soc.* **2012**, *134*, 7580−7583.
(72) Ertem, M. Z.; Konezny, S. J.; Araujo, C. M.; Batista, V. S. Functional Role of Pyridinium during Aqueous Electrochemical Reduction of $CO_2$ on Pt(111). *J. Phys. Chem. Lett.* **2013**, *4*, 745−748.